Numerical Modeling of the Cold Spray Process

Qing Song Zhu

A Thesis

in

The Department

of

Mechanical & Industrial Engineering

Presented in Partial Fulfillment of the Requirements
For the Degree of Master of Applied Science at
Concordia University
Montreal, Québec, Canada

December 2006

© Qing Song Zhu, 2006

Library and
Archives Canada

Published Heritage
Branch

395 Wellington Street
Ottawa ON K1A 0N4
Canada

Bibliothèque et
Archives Canada

Direction du
Patrimoine de l'édition

395, rue Wellington
Ottawa ON K1A 0N4
Canada

NOTICE:
The author has granted a non-
exclusive license allowing Library
and Archives Canada to reproduce,
publish, archive, preserve, conserve,
communicate to the public by
telecommunication or on the Internet,
loan, distribute and sell theses
worldwide, for commercial or non-
commercial purposes, in microform,
paper, electronic and/or any other
formats.

The author retains copyright
ownership and moral rights in
this thesis. Neither the thesis
nor substantial extracts from it
may be printed or otherwise
reproduced without the author's
permission.

AVIS:
L'auteur a accordé une licence non exclusive
permettant à la Bibliothèque et Archives
Canada de reproduire, publier, archiver,
sauvegarder, conserver, transmettre au public
par télécommunication ou par l'Internet, prêter,
distribuer et vendre des thèses partout dans
le monde, à des fins commerciales ou autres,
sur support microforme, papier, électronique
et/ou autres formats.

L'auteur conserve la propriété du droit d'auteur
et des droits moraux qui protège cette thèse.
Ni la thèse ni des extraits substantiels de
celle-ci ne doivent être imprimés ou autrement
reproduits sans son autorisation.

In compliance with the Canadian
Privacy Act some supporting
forms may have been removed
from this thesis.

While these forms may be included
in the document page count,
their removal does not represent
any loss of content from the
thesis.

Conformément à la loi canadienne
sur la protection de la vie privée,
quelques formulaires secondaires
ont été enlevés de cette thèse.

Bien que ces formulaires
aient inclus dans la pagination,
il n'y aura aucun contenu manquant.

Canada

Abstract

Numerical Modeling of the Cold Spray Process

Qing Song Zhu

This thesis involves numerical modeling of several cold spray processes in order to predict the gas flow as well as the particle conditions upon impacting on a substrate. Particle normal velocity was found to be the most important factor to improve the deposition efficiency and coating quality. Particle velocity was calculated with both Lagrangian and Eulerian approaches. The Lagrangian approach was used to investigate the effect of particle size and substrate geometry in a dilute particle flow. The shape and strength of the bow shock formed near the substrate for different geometries (such as concave, convex, and flat) were studied. Consequently, the particle normal velocities impacting on the substrates located at various stand-off distances were calculated. Furthermore, the numerical simulations were repeated with particles of various sizes as well as different types of feeding gas. The results were compared to obtain the optimum substrate location and the appropriate particle size for each feeding gas. The numerical results were validated against the experimental results for the majority of the process parameters including the gas Mach number and mean particle velocity. The Eulerian approach was also implemented to model dense particulate flows. It was found that a dense particulate flow could significantly decelerate the gas flow and consequently result in small particle velocity.

Acknowledgement

I would like to thank my supervisor Professor Ali Dolatabadi for his continuous guidance throughout this research, especially for his support and encouragement whenever I encountered a difficulty.

I would also like to thank my colleagues at the CFD Lab of Concordia University, in particular, Mrs. X. X. Hu, S. Arabzadeh, and Mr. A. Arzpeyma, M. movassa, B. Sanderse, B. Samareh, V.R. Srivatsan. They have helped me a lot in technical problems and in English.

I also wish to express my appreciation to my wife and my child for their support.

Table of Contents

List of Figures

viii

ix

List of Tables

Nomenclature

A	cross-sectional area of the particle
c	turbulent model constant
c_m	speed of sound of material m
c_v	constant volume specific heat
C_D	drag coefficient
d	particle diameter
e	internal energy
E	total energy
F_b	body force
$\vec{g}$	gravity
h_c	convective heat transfer coefficient
H	total enthalpy
k	turbulent kinetic energy

k	isentropic coefficient
K_{12}	inter-phase momentum exchange coefficient
m	mass
Ma	Mach number
p	pressure
P	production rate of turbulent kinetic energy
R	gas constant
R_e	Reynolds number
R_{12}	inter-phase heat exchange coefficient
S	source term
t	time
T	temperature
u,v,w	velocity components in x,y,z-directions
$\vec{U}$	velocity vector
V	volume

Greek symbols

α_m	volume fraction of material m
γ	specific heat ratio

δ_{ij}	Kronecker delta
ε	rate of dissipation of turbulent energy
Γ	diffusion coefficient
λ	thermal conductivity
μ	molecular viscosity
μ_{eff}	effective viscosity
ρ	density
θ_m	expected volume fraction of material m
σ	turbulent model constant
τ_F	fluid time characteristic
τ_R	particle response time

Subscripts

BK	back cell face
FR	front cell face
g	gas
k	turbulent kinetic energy
m	material type

o	pure material
L	left cell face
p	particle
R	right cell face
t	turbulent
ε	rate of dissipation of turbulent energy

Superscripts

*	quantities that have interpolated from cell-center to face-center
c	cell-centered quantity
e	edge location
f	face-centered quantity
L	Lagrangian value
n	current time step

1. Introduction

Thermal spray is a class of processes to deposit accelerated and heated coating material on a substrate. The coating material can be metallic, such as copper, titanium, and aluminum or nonmetallic, such as ceramics, glasses, and polymers. The coating material is normally in the form of fine powder, which can be easily heated to molten state and accelerated to high velocity. There are also other forms of coating material, such as wire, ceramic-rod, and molten materials which are widely used. To be successfully deposited on a substrate, the coating material must either obtain high kinetic energy from the gas flow, or absorb sufficient thermal energy from heat sources, such as an Oxy-Fuel flame or an electric arc. If the kinetic energy of the coating material is not high enough, the coating material has to be heated to semi molten or molten state to facilitate the coating process, as in a plasma or HVOF process. On the contrary, if the coating material is accelerated to high velocity, it can even be deposited at room temperature, as in a cold spray process.

Thermal spray technology is widely used in various industries to form a coating which can prevent work pieces from wear, corrosion, erosion, and heating. It is also used to produce engineered materials with unique properties, such as strain-tolerant ceramics, metallic glasses, cermets, and metal-polymer composites (plastimets).

1

Based on the way of heating and the type of the coating material, thermal spray processes can be divided into the following categories: molten metal flame spray, power flame spraying, wire flame spraying, ceramic rod flame spraying, detonation flame spraying, high velocity oxy-Fuel spraying (HVOF), nontransferred plasma arc spraying, electric arc spraying, RF plasma spraying, and cold spray.

Some of these thermal spray technologies, such as molten metal flame spray, have been developed over a century. In general, the trend in the development of thermal spray processes has been directed toward reducing the gas flow temperature. The commonly used thermal spray systems are listed in the following sections, involving plasma spraying, high velocity oxy-fuel (HVOF), and cold spray process.

1.1.　Common Thermal Spray Processes

Plasma Spraying

Plasma spraying is a thermal spray process using an electric arc to heat and ionize a gas stream into a plasma gaseous cloud which melts the coating material and propels it to the substrate [1]. Plasma spraying technology was commercially developed in the 1950s.

Figure 1-1 shows a schematic diagram of a typical plasma spray process. A gas flow is fed into a plasma spray gun and heated to form plasma, a compound of free electrons, positive ions, neutral atoms and molecules produced from the ionized gas. Various gases can be used in a plasma spray process, such as argon, nitrogen, hydrogen, and helium. To obtain a plasma flow with satisfactory velocity and temperature, a mixture of gases, such as argon-hydrogen, argon-helium or nitrogen-hydrogen, is also

2

widely used. The feed gas is heated by an electric arc which is initiated by a high voltage

discharge between a water cooled copper anode and a tungsten cathode. The temperature

of the heated gas is extremely high (ranging from 5000 °C to 16000 °C) in the area of the

electric arc that the chemical bonds of the gas molecules and atoms are broken,

consequently resulting in the formation of plasma, an ionized gaseous compound. Since

the anode is shaped as a nozzle, the plasma flame is accelerated in this nozzle. When the

coating material, which is normally in the form of powder, is injected upstream into the

nozzle bore, the plasma flame melts the powders and transports them toward the substrate

to form a coating. The spray distance, known as the stand-off distance of the substrate,

varies within a range of 25 to 150 mm.
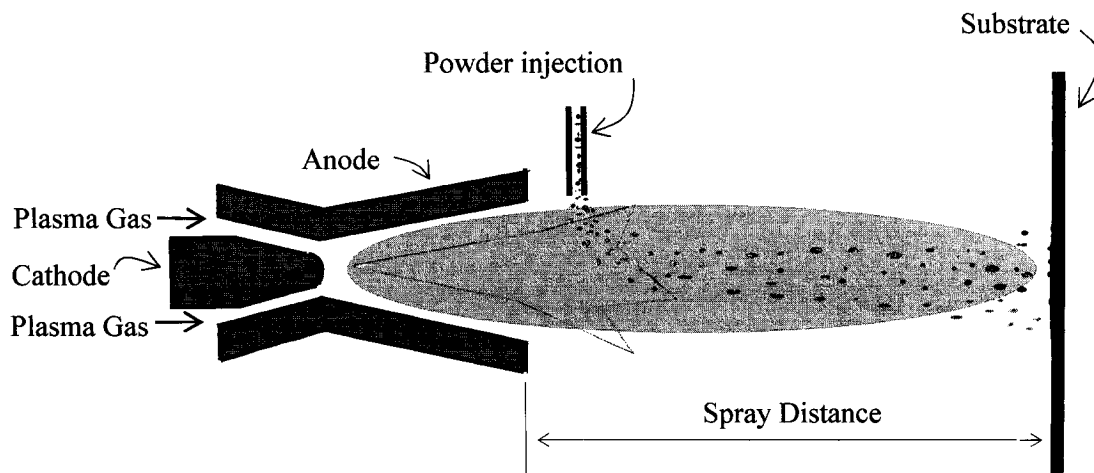
Figure 1-1   Schematic diagram of the plasma spray process

One of the advantages of plasma spraying system is that the plasma guns can be

simply designed and manufactured. Moreover, as the temperature of a plasma stream can

be as high as 16,000 °C, plasma spraying systems can be used to coat refractory metals,

3

such as tungsten, as well as ceramics, such as zirconia. Most feedstock materials used in thermal spray processes can be coated by plasma spraying systems. However, a high temperature results in some disadvantages, such as high level of oxidation in the coating and high porosity in the coating structure. Additionally, the residual stresses through the coating are rather high leading to cracks forming. In order to reduce oxidation and residual stress, new coating methods were developed, such as high velocity oxy-fuel spraying (HVOF), in which coating process is performed under a lower temperature which results in a higher particle velocity compared to a plasma spray.

High Velocity Oxy-Fuel Spraying (HVOF)

High velocity oxy-fuel spraying (HVOF) is a flame spray process involving high velocity gas and particle flow [2]. It was developed in the 1980s based on the rocket engine technologies.

As shown in Figure 1-2, a mixture of oxygen and fuel is fed into the inlet of the converging-diverging nozzle, known as de Laval nozzle, and burns. Various gases can be used as the fuel in HVOF process, such as hydrogen, propane, propylene, and kerosene. Heat and by-products are produced from the combustion process of the gas mixture. The gas products which are under high pressure (6 atm) and high temperature (about 3000K) accelerate in the converging part of the nozzle. At the nozzle throat, the gas Mach number is about 1. The gas expands further in the diverging section of the nozzle and develops into a supersonic flow. A series of diamond-shaped shocks are produced near the nozzle exit when the gas flow interacts with the boundary of the surrounding atmosphere. These shocks are also referred to as "shock diamonds", which are composed

4

of sequence of compressive oblique shocks and Prandtl –Meyer expansion waves. The physics of shock diamonds will be further explained in the second chapter of this thesis.
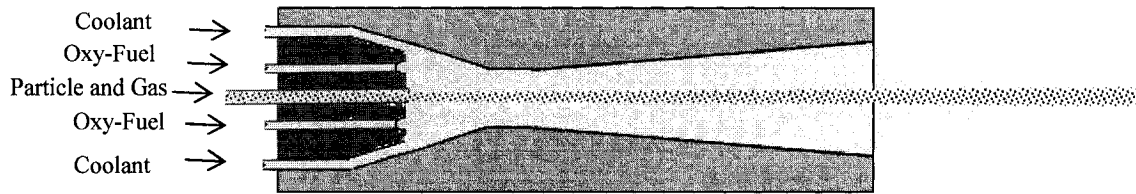
Figure 1-2 Schematic of a HVOF nozzle

Powders are also injected axially into the converging section of the nozzle, where they are propelled and heated by the expanding hot gases. They are accelerated continuously through the nozzle. However, they are decelerated by the shock diamonds and the bow shock between the nozzle exit and the substrate. Finally, the particles impact on the substrate and form a coating.

The gas temperature in an HVOF process (about 3000K) is lower than that of a plasma spraying process (about 10,000K). Therefore, the gas density and consequently particle velocity is much higher in an HVOF process compared to those of a plasma spray (about 500 m/s for HVOF and 100 m/s for plasma). This results in a dense and low porosity coating when it compares with that of the plasma spraying system. The disadvantages of HVOF technology include low deposition efficiency and moderate to high level of oxidation in the coatings.

High temperature in the conventional thermal spray processes, such as plasma spraying or HVOF, results in oxidation, porosity and thermal stresses in the coating layer. The general trend in development of thermal spray technology is to reduce the gas temperature, and to increase the particle velocity upon impact on the substrate. Cold gas

5

dynamic spray, or "cold spray" for short, is a breakthrough of the conventional thermal spray process because it can deposit particles with high velocity at room temperature [3].

1.2.   Cold Spray

Cold spray is a thermal spray process in which fine particles (typically between 1-50 μm) are accelerated by a supersonic gas flow to a high velocity (ranging from 500 up to 1500 m/s), then impact on a substrate, plastically deform, fuse and consolidate to form a coating [3]. The particles used in the cold spray process are not preheated to a molten condition. The gas temperature in this process is relatively low (300-1000K) [4]. Cold spray can even be performed under room temperature.

Cold spray technology was developed by Papyrin et al. [3] in mid 1980s at the Institute of Theoretical and Applied Mechanics of the Russian Academy of Sciences. Because this process generally is performed at room temperature, there is no oxidation forming in the coating. As a result, this technology garnered the interests of researchers world wide. Over the last decade efforts have been made to commercialize this technology.

As shown in Figure 1-3, a cold spray system is basically composed of a converging-diverging de Laval nozzle, a powder feeder, a high pressure gas tank and a gas heater. The highly compressed gas expands and accelerates in the nozzle, developing a supersonic flow in the diverging section of the nozzle [5]. The particles are also injected into the nozzle inlet, where they are propelled and accelerated by the gas flow. At the nozzle exit, the particle velocity may exceed 1200 m/s when a combination of helium and fine particles are used.

6

Shock Diamonds   Bow Shock

Powder Feeder

Compressed Gas

Gas Heater
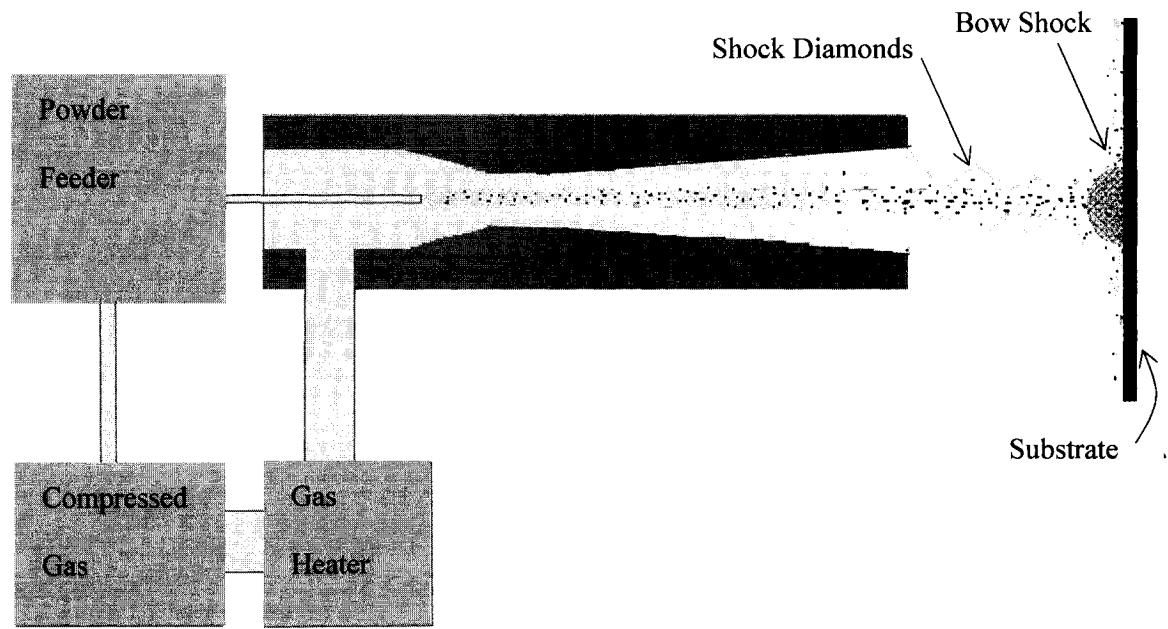
Substrate

Figure 1-3   Schematic of a cold spray system

Outside the nozzle, coating particles are further accelerated by the shock diamonds. After that, coating particles pass through a strong bow shock near the substrate. As a result, their velocities decrease dramatically. Only those particles having a velocity larger than the critical velocity [6] can successfully be deposited on the substrate. The critical velocity is the minimum velocity required for a particle in order to be successfully deposited on a substrate.

Low temperature in cold spray process results in a reduced level of coating oxidation, which is one of the main benefits of cold spray process versus the other thermal spray processes. The electrical conductivity of the coated materials by cold spray technology is also high because of the low level of oxidation associated with cold spray coatings. Besides this, some other benefits are obtained from this low temperature coating technology, such as reduced material loss by vaporization, low residual stress, improved

7

phase and compositional stability, insignificant grain growth and recrystallization, etc. Furthermore, the range of metal powders which can be coated is wider in the cold spray process, including thermally sensitive alloys and small powders.

Other advantages of cold spray stem from the high impact velocity of the particles, such as high deposition rate, the improved adhesion, low gas entrapment and porosity, high density of the coated materials, increased bond strength, reduced masking requirements, improved surface finishes and lower heat input to work pieces.

One limitation of cold spray process is that the coating material has to be ductile owing to the principle of impact-fusion coating build-up of this process. Various ductile metals, alloys, and polymers can be used in cold spray process, such as Zn, Sn, Ag, Cu, Al, Ti, Nb, Mo, Nicr, Cu-Al, Nickel alloys, and MCrAlYs. Brittle metals or ceramics cannot be easily coated by cold spray technology, except being mixed with a ductile material.

Moreover, the work piece material has to be strong enough to withstand the erosion effect of the high speed particles. The soft or friable substrates are not appropriate to be used in a cold spray process. Other disadvantages of the cold spray process include high gas pressure, short lifetime of key components and high gas cost because of the use of high gas flows.

Based on the improved wear and fatigue characteristics associated with cold sprayed coating layers, the process can be widely used in industries to make a protective coating layer on a substrate, preventing the substrate from corrosion, erosion, heating, and wear. It can also be used for some special purposes, such as depositing electrical conductors and solders, and coating a metal layer on a ceramic or glass substrate.

8

Potential applications of cold spray technology have been found in various industries, such as automotive, aerospace, electronics, biomedical, chemical, mineral processing, paper, petroleum, glass, and power generation. It can also be used as a technique to fabricate small parts layer by layer, to weld in low-temperature, to join chemically dissimilar materials, to provide electrical insulation for the work pieces, or to produce new materials, such as metallic glasses, cermets, metal-polymer composites (plastimets), and nano-structured materials.

Although the potential application of cold spray technology is vast, as a newly emerged technology, cold spray technology has still not been fully understood and commercialized because of the technological and numerical challenges associated with this process described below.

1.3. Motivation

1.3.1. Technological Challenge

The main challenge to commercialize the cold spray technology is to increase the particle deposition efficiency (*DE*). Deposition efficiency is defined as:

$$DE = \frac{mass\ of\ particles\ deposited\ on\ a\ substrate}{mass\ of\ particles\ fed\ to\ the\ nozzle}$$

The deposition efficiency of any actual cold spray process is not satisfactory (normally less than 50%). This is because the velocities of many particles upon impact on a substrate are less than the critical velocity.

9

Critical Velocity

It was found that the particle velocity upon impact on a substrate has to exceed a critical value for successful deposition of the particles in the cold spray process. Critical velocity varies according to some factors, such as particle material, substrate material, and particle temperature.

As shown in Figure 1-4, the critical velocity for copper particle is about 500 m/s. The velocity of the particles must be greater than 500 m/s for copper particles to get a chance to be deposited on the substrate. When the particle velocity exceeds the critical velocity, further increasing the particle velocity will improve the coating deposition efficiency and quality. It can be concluded that the deposition efficiency has more or less a linear relationship with the particle velocity upon impact.

According to the research of Li et al. [6], the tangential velocity of a particle upon impact on a substrate has a negligible influence on deposition. The particle velocity in Figure 1-4 should be the normal particle velocity upon impact on the substrate. In our research, the mean normal velocities of 1000 particles are calculated. The mean normal velocity is used to evaluate the level of deposition efficiency. The method to calculate the normal velocity upon impact will be described in the second chapter of this thesis.

10

Copper Particle on Stainless Steel Substrate
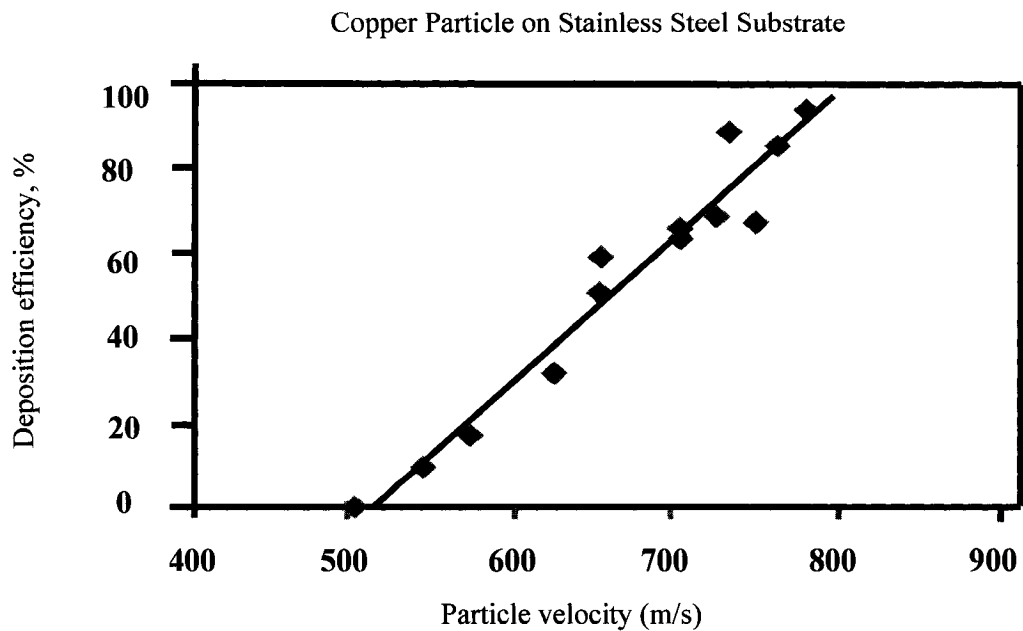
Figure 1-4   Relationship between particle velocity and deposition efficiency (from [7])

1.3.2.   Numerical Challenge

As a two-phase compressible turbulence flow, the gas flow in a cold spray process is a challenging problem to be simulated with a simple model. The model should be capable of estimating the properties of the gas flow, such as the gas temperature, pressure, and velocity by solving the Navier-Stocks equations, and predicting the properties of the particles, such as the particle temperature and velocity by evaluating particle-gas and particle-particle interactions. However, this ideal model would exceed current computational capabilities. Therefore, two approximate models are used in the present work, one is the Lagrangian Model [8 and 9], and the other is the Eulerian Model [10 and 11].

The nature of fluid-particle flow, dilute or dense [12], determines which model should be used for a specific cold spray flow. The particle-particle interactions can be

11

neglected in a dilute particle flow. The Lagrangian approach is appropriate for simulating dilute particle flows. However, in a dense flow these interactions can significantly affect the gas phase and the particle velocity. In this case the Eulerian approach can capture most of the physics governing the two-phase flow. The flow regime for any specific case can be determined by evaluating the scaling parameters, such as Stokes number, loading and volume fraction, which are described below:

Stokes Number

The Stokes number is the ratio of particle response time τ_R to a time characteristic of the fluid motion τ_F [13].

$$St = \frac{\tau_R}{\tau_F} = \frac{\rho_P d^2 U}{18 \mu L} \tag{1.1}$$

where U, L, and μ are the characteristic fluid velocity, a length scale, and fluid viscosity, while, ρ_p and d, are the particle density and diameter.

When the Stokes number of the particles is small (St<<1), particles will move with the gas turbulent motion of gas phase (i.e. dilute flow). On the contrary, when the Stokes number of the particles is large (St>>1), there is a velocity difference between the particles and the gas phase. In this case the particles motion will augment the turbulence of the gas phase. Further more, the particle-particle collision will be too significant to be neglected. Consequently, the flow should be treated as a dense flow.

Loading

Loading and volume fraction are important scaling parameters to evaluate the effect of the dense flow in the two-phase flow problems. Loading is the ratio of the mass flows of the dispersed phase to that of the continuous phase.

12

$$Loading = \frac{mass\ flow\ of\ the\ dispersed\ phase}{mass\ flow\ of\ the\ continous\ phase}$$

Volume Fraction

As presented in equation (1.2), the volume fraction θ is the ratio of the volume of the particles occupied in a control volume to the volume of the control volume (Figure 1-5).

$$\theta_d = \frac{\sum V_p}{V} \tag{1.2}$$
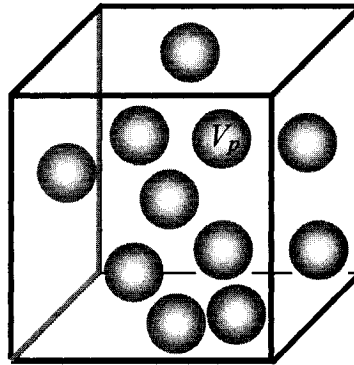
Figure 1-5   Particle volume fraction

The gas-particle flow regimes can be identified based on the Stokes number and the volume fraction as shown in Figure 1-6 [14]. When particle volume fraction is less than 10^{-6}, the effect of particle motion on the gas turbulence can be neglected. When particle volume fraction is between 10^{-6} and 10^{-3}, the particles motion can either augment gas turbulence or decrease it, depending on the Stokes number. When the particle volume fraction is greater than 10^{-3}, particle-particle interactions and collisions are significant. In this case, the particle-gas flow should be considered as a dense flow.

13

In this thesis the Lagrangian approach [8], [9] and the Eulerian approach [10], [11] were used to analyze the cold spray process. Both models have their strengths and short comings. The Lagrangian model treats the particles as discrete entities. Since the Lagrangian model neglects the particle-particle collisions in the two-phase flow, it can be used to simulate the dilute particle flow, in which the surface and body forces are the dominant forces on the particles. The Eulerian Model treats the particles as a continuum phase. Since the Eulerian model is capable of predicting the particle-particle interactions and collisions, it can be used to estimate the dense particle flow, in which the particle-particle interactions are significant.
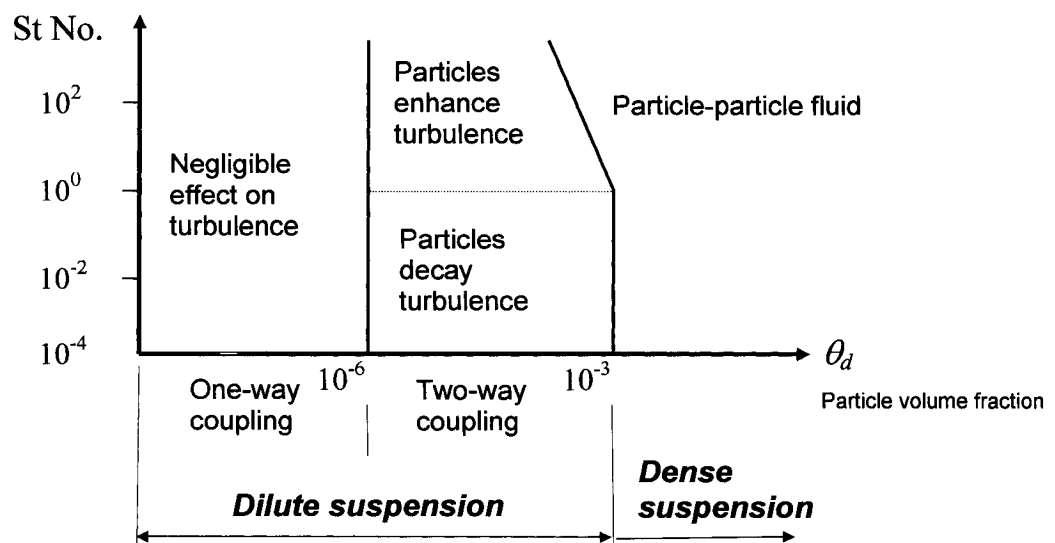
Figure 1-6   **Proposed map for modulation of fluid-particle flows (from [14])**

In the past few years, more and more efforts have been made by using the above mentioned approaches to face the technical and numerical challenges of cold spray technology.

14

1.4. Previous Studies

The studies in the early stages of the development of cold spray process included the jet gas dynamics, physics of plastic deformation during splat-to-substrate impact, spray nozzle configurations, range of coating materials, and properties of the coated materials.

Papyrin et al.[3] designed the first cold spray system using a de Laval nozzle, a gas heater, a high pressure gas supply, a metering powder feeder , and a powder particle flow controller. A patent was issued in the United States in 1994 titled as "Gas-dynamic spraying method for applying a coating". Experiments were conducted in his study with various particles, such as aluminum, zinc, tin, copper, nickel, titanium, iron, vanadium, cobalt, and metal alloys, and with various carrier gases, such as air, nitrogen, helium, and gas mixture. The deposition efficiency was measured for various air temperature, pressure, and particle velocity. The range of nozzle dimension, gas temperature and pressure, gas flow rate, powder flow rate and particle size were suggested in the patent. A balance between particle size, density, temperature, and velocity was found important to achieve the desired coating.

Experiments and simulations were conducted by Stoltenhoff et al. [15] in order to investigate the effects of process parameters, such as gas pressure and temperature at the nozzle inlet, on the deposition efficiency. The relationship between velocity of the coating particles at the nozzle exit and the gas temperature or the gas pressure at the nozzle inlet was demonstrated. However, the particle normal velocity upon impacting on a substrate was not addressed.

15

The sensitivity of a cold spray process to Mach number was explored by Jodoin [16]. It was found that the flow Mach number in a cold spray process should not exceed 3 because of the strong shock-particle interactions. On the other hand, the Mach number should not be lower than 1.5 to avoid the negative effect of high temperature on the substrate.

In order to improve the deposition efficiency of the cold spray process, recently many research has been conducted focusing on the effect of particles size, impact velocity, aerosol physics, substrate geometry, substrate stand-off distance and particle-shock interactions [14].

An optimal design of a cold spray nozzle for internal coatings was achieved by Li et al. [17] by studying the effect of the nozzle expansion ratio, particle size, carrier gas type, operating pressure and temperature on the behavior of spray particles. A group of nozzles with various exit diameters, ranging from 2 to 8 mm, were used in the simulation. A nozzle with an exit diameter of 5 mm was found to be the optimal one to achieve the highest particle velocity. It was also found that when the gas temperature and pressure were increased, a higher particle velocity was obtained. Particles velocity could be further increased if helium is used as the carrier gas. The effect of particle size was also studied in this paper. Small particles, especially those particles less then 20 μm, were confirmed appropriate to be used in the limited space. However, the exact optimum particle size was not addressed in this work.

Several cold spray variables were investigated in the study of Han et al. [18] through 3-D computational modeling and experiments. The shape of the nozzle exit used

16

in this research was rectangular. The deposition efficiency was found improved when the inlet gas temperature and pressure were increased. It was also found that the buildup of particles inside the nozzle could significantly affect coating formation because the particle velocity was reduced. Nozzles with larger throat area were suggested to be used for coating hard alloy powder or for a large powder feed rate. It was observed that high powder carrier gas flow rate results in low deposition efficiency because the temperature of the carrier gas was lower than that of the heated main gas flow. The effect of the stand-off distance on deposition efficiency was demonstrated. The highest deposition efficiency in this study was reported as about 40% when the substrate stand-off distance was 10 mm. However, it was not shown how the deposition efficiency would change if the stand-off distance is further reduced in the experiment.

Dolatabadi et al. [10, 19, 20, 21, and 22] addressed the physics of high speed particle-laden flow in HVOF and cold spray processes. Two numerical models, the Lagrangian approach [8 and 9] and the Eulerian-Eulerian approach [10 and 11] were used to model the HVOF spray process and cold spray process. In the studying of the HVOF process, the effect of mesh size to the simulation result and the effect of diamond shock to the particle velocity were analyzed [10] [21]. A shroud was designed to be attached to the outlet of the supersonic nozzle, which can significantly reduce the particle oxidation in the thermal spray processes. His work shed light on the direction of further study of cold spray process.

According to the above mentioned studies, improving the deposition efficiency of cold spray processes requires an increase in the particle velocity. This in turn, is

17

influenced by various factors, such as the design of the nozzle, the stagnation pressure and temperature of the gas, the particle and gas material, the particle size, the substrate location, and the substrate geometry. Experiments have been conducted to study the effect of the particle size and spray angle [6]. However, the effects of the substrate shape and the resultant bow shock near the substrate have not been fully understood.

1.5.   Objectives

Since the factors which affect the deposition efficiency and coating quality are very important for utilizing the cold spray technology by industry, the objective of this research is to find out a numerical model to further understand the process and to analyze the effects of key parameters. This numerical model should be capable of working as a design tool to simulate the cold spray process in order to improve deposition efficiency and coating quality in the cold spray process.

The objectives of this research are:

- Study the effect of shock diamonds and the bow shock on particle impact velocity

- Estimate the optimum substrate location for a specific operating condition

- Predict the optimum particle size for a given operating condition

- Analyze the effect of substrate geometry on the normal particle velocity upon impact

- Study the effect of dense particle flow on the gas phase

- Study the effect of dense particle flow on particle velocity

- Study the effect of particle density in a dense particle flow

1.6.   Thesis Organization

The organization of the thesis is as follows: Chapter 1 introduces some typical thermal spray processes and the previous studies on cold spray. Moreover, the technical and numerical challenges in the research of cold spray and the objectives of this thesis are presented. In Chapter 2, the Lagrangian method is used to analyze the gas phase and particles conditions in the cold spray process. The effect of the bow shock is analyzed with two different drag coefficient models. Furthermore, the optimum substrate location and particle size are presented. Comparisons of the normal particle velocity are made for two different carrier gases (helium and nitrogen). Finally, the effect of the substrate geometry is analyzed. Chapter 3 describes the methodology and the results of the Eulerian approach. The effect of particle volume fraction on the gas flow and the particle velocity is presented. The effects of the bow shock and particle density in the dense particle flow are also demonstrated. Finally, conclusions are summarized and future works are recommended in chapter 4.

19

2.   Lagrangian Approach

In this chapter, the Lagrangian approach [8 and 9] is used to analyze the effect of shocks, substrate and particle size on the mean particle velocity upon impact in the cold spray process. The gas phase is solved in the Eulerian frame, while the particles are treated as discrete entities and solved by the Lagrangian particle tracking approach. Based on the predetermined properties of the surrounding gas phase, the particle mass, velocity and temperature are calculated simultaneously. The interaction between the particulate phase and the continuous phase is considered by using a two-way coupling model. The particle volume fraction is neglected.

2.1.   Governing Equations

2.1.1.   Continuous Phase

The flow of cold spray is viscous, compressible, and turbulent. The governing equations include the equations of continuity, momentum, and energy. Ideal gas state equation is also used to close the system of equations.

20

Continuity equation

$$\frac{\partial \rho}{\partial t} + \frac{\partial (\rho u_j)}{\partial x_j} = 0 \tag{2.1}$$

Momentum equations

$$\frac{\partial}{\partial t}(\rho u_i) + \frac{\partial}{\partial x_j}(\rho u_j u_i) = -\frac{\partial p}{\partial x_i} + S_{u_i} + \frac{\partial}{\partial x_j}\left\{ \mu_{eff}\left(\frac{\partial u_i}{\partial x_j} + \frac{\partial u_j}{\partial x_i}\right) - \frac{2}{3}\mu_{eff}\frac{\partial u_l}{\partial x_l}\delta_{ij} \right\} \tag{2.2}$$

Energy equation

$$\frac{\partial}{\partial t}(\rho H) + \frac{\partial}{\partial x_j}(\rho u_j H) - \frac{\partial p}{\partial t} = \frac{\partial}{\partial x_j}\left(\lambda \frac{\partial T}{\partial x_j} + \frac{\mu_t}{Pr_t}\frac{\partial h}{\partial x_j} \right) + S_E +$$

$$\frac{\partial}{\partial x_j}\left\{ u_j\left[\mu_{eff}\left(\frac{\partial u_i}{\partial x_j} + \frac{\partial u_j}{\partial x_i}\right) - \frac{2}{3}\mu_{eff}\frac{\partial u_l}{\partial x_l}\delta_{ij} \right] + \mu \frac{\partial k}{\partial x_j} \right\} \tag{2.3}$$

Equation of state

$$p = \rho RT \tag{2.4}$$

where $\mu_{eff} = \mu + \mu_t$, $H = h + \frac{1}{2}(u_i u_i) + k$, λ and k are the effective viscosity, the total

enthalpy, the thermal conductivity, and the turbulent kinetic energy, respectively. The

source terms, S, in the momentum and the energy equations provide a two-phase coupling

between the gas phase and the particles.

Viscous Model

The Reynolds stress model is used in this work as the viscous model [23], [24]. The

Reynolds stress transport equations can be derived by multiplying the exact momentum

equations with a fluctuating property. The product then has to be Reynolds-averaged.

21

The variables in Reynolds averaging can be decomposed into two parts, the emsemble-averaged mean and the fluctuating components.

$$\phi = \overline{\phi} + \phi'$$ (2.5)

where $\overline{\phi}$ presents the time-averaged mean of a variable, such as velocity, pressure, energy, or species concentration. ϕ' denotes the fluctuating components of the variable. The ensemble-averaged momentum equations are yielded by substituting the Reynolds-averaged variables into the instantaneous continuity and momentum equations, and can be written in Cartesian tensor form as the follows:

$$\frac{\partial}{\partial t}(\rho u_i) + \frac{\partial}{\partial x_j}(\rho u_j u_i) = -\frac{\partial p}{\partial x_i} + S_{u_i} + \frac{\partial}{\partial x_j}\left\{\mu_{eff}\left(\frac{\partial u_i}{\partial x_j} + \frac{\partial u_j}{\partial x_i}\right) - \frac{2}{3}\mu_{eff}\frac{\partial u_l}{\partial x_l}\delta_{ij}\right\}$$ (2.6)

$$\text{where } S_{u_i} = \frac{\partial}{\partial x_j}\left(-\rho\overline{u_i' u_j'}\right)$$ (2.7)

The Reynolds stresses, $-\rho\overline{u_i' u_j'}$ in Equation (2.7) represent the effects of turbulence. These stresses are modeled in order to close the Reynolds-averaged momentum equation [23].

2.1.2. Dispersed Phase

The Lagrangian particle-tracking approach is used to simulate the motion of the particles. Some assumptions are made to simplify the calculation. For example, the

22

particles are assumed to be solid, spherical, and inert. The volume fraction of the particles is neglected.

The equation used to calculate the velocity and the position of the particles is [25]:

$$m_p \frac{d\vec{U}_p}{dt} = \frac{1}{2} \rho_g A_p C_D \left(\vec{U}_g - \vec{U}_p \right) \left| \vec{U}_g - \vec{U}_p \right| + \vec{F} \qquad (2.8)$$

where m_p is the mass of particle, $\vec{U}_p$ and $\vec{U}_g$ are the instantaneous particle and gas velocities, respectively. ρ_g is the density of the gas. A_p is the cross-sectional area of the particle and $\vec{F}$ denotes external forces such as gravity. Particle velocity can be obtained by integrating equation (2.8) for one time step. The particle position can be derived by further integrating this equation over the time step.

The particle drag coefficient, C_D, is an important factor in equation (2.8) which significantly influences the accuracy of the computational simulation of the coating particles' motion. C_D is found to be either a function of the particle Reynolds number ($C_D = f(\text{Re}_p)$), such as the correlation of Igra and Takayama [26], or a function of both the particle Reynolds number and the Mach number ($C_D = f(Ma_p, \text{Re}_p)$), such as the correlation of Henderson [27]. The particle Reynolds number, Re_p, and Mach number, Ma_p, are defined by equations (2.9) and (2.10).

$$\text{Re}_p = \frac{\rho_g \left| U_g - U_p \right| D_p}{\mu_g} \qquad (2.9)$$

$$Ma_p = \frac{\left| U_g - U_p \right|}{\sqrt{kRT_g}} \qquad (2.10)$$

23

In this thesis, the interaction between the particles and the gas phase was studied by using both the correlation of Igra and Takayama [26] and the correlation of Henderson [27].

Igra and Takayama Correlation

The correlation of Igra and Takayama [26] presented in equation (2.11) covers a range of Reynolds number from 200 to 101,000.

$$\log C_D = 7.8231 - 5.8137 \log \text{Re}_p + 1.4129 (\log \text{Re}_p)^2 - 0.1146 (\log \text{Re}_p)^3 \qquad (2.11)$$

Henderson Correlation

$$C_D = \begin{cases} \left\{ 24 \left(\text{Re}_p + (\gamma/2)^{1/2} Ma_p \left\{ 4.33 + \left(\dfrac{3.65 - 1.53 T_p/T}{1 + 0.353 T_p/T} \right) \exp\left[-0.247(2/\gamma)^{1/2} \dfrac{\text{Re}_p}{Ma_p} \right] \right\} \right) \right)^{-1} \\ \\ + \exp\left(-\dfrac{0.5 Ma_p}{\text{Re}^{1/2}} \right) \left[\dfrac{4.5 + 0.38 \left(0.03 \text{Re}_p + 0.48 \text{Re}_p^{1/2} \right)}{1 + 0.03 \text{Re}_p + 0.48 \text{Re}_p^{1/2}} + 0.1 Ma_p^2 + 0.2 Ma_p^8 \right] + \\ \\ 0.6(\gamma/2)^{1/2} Ma_p \left[1 - \exp\left(-\dfrac{Ma_p}{\text{Re}_p} \right) \right] \qquad \qquad \qquad \text{for } Ma_p <= 1 \\ \\ \dfrac{0.9 + \dfrac{0.34}{Ma_p^2} + 1.86 \left(\dfrac{Ma_p}{\text{Re}_p} \right)^{1/2} \left[2 + \dfrac{4}{\gamma Ma_p^2} + 1.058 \dfrac{1}{Ma_p} \left(\dfrac{2T_p}{\gamma T} \right)^{1/2} - \dfrac{4}{\gamma^2 Ma_p^4} \right]}{1 + 1.86 \left(Ma_p / \text{Re}_p \right)^{1/2}} \qquad \text{for } Ma_p >= 1.75 \\ \\ C_D(1.0, \text{Re}_p) + (4/3)(Ma_p - 1) \left[C_D(1.75, \text{Re}_p) - C_D(1.0, \text{Re}_p) \right] \qquad \text{for } 1 < Ma_p < 1.75 \end{cases}$$

$$(2.12)$$

Henderson correlation [27] covers all flow regimes, from subsonic flow to supersonic flow. Given by equation (2.12), Henderson correlation includes three parts according to the particle Mach number Ma_p.

24

Each correlation has its strong points and limitations in the simulation of the particle motion in the cold spray process. The discrepancy between these two correlations are compared and demonstrated in the results and conclusion section.

User defined functions (UDF) are written with C language in order to take into account the effect of the particle drag coefficient. The drag force between particles and fluid is defined by the following equation:

$$F_D = \frac{18\mu}{\rho_p D_p^2} \frac{C_D \, \text{Re}}{24} \tag{2.13}$$

where ρ_p is the particle density, D_p denotes the particle diameter. The particle drag coefficient, C_D, is substituted by the correlations of Igra and Takayama [26] and Henderson [27], respectively. The drag force, F_D, calculated by equation (2.13) is returned to the solver of the discrete phase model in Fluent. After compiling, these UDFs are hooked to the Fluent codes. Consequently, the particle velocity is calculated based on the new drag correlations defined by the UDF file. The results are presented in the results and conclusions section.

Particle Temperature

The temperature distribution inside each particle is assumed uniform (lumped capacitance system). To simplify the calculation of particle temperature, the radiative heat transfer is neglected. The particle temperature can be obtained by integrating the energy equation as follows:

$$m_p C_p \frac{dT_p}{dt} = A_p h_c (T_g - T_p) \tag{2.14}$$

25

where C_p is the specific heat of the particle, and h_c is the convective heat transfer coefficient. The convective heat transfer coefficient, h_c, can be expressed as follows:

$$h_c = \frac{Nu\ \lambda}{d_p}$$

(2.15)

The Nusselt number is given by equation (2.16):

$$Nu = 2.0 + 0.6\,Pr^{0.33}\,Re^{0.5}$$

(2.16)

where Pr is the Prandtl number and Re is the Reynolds number.

2.2.   Numerical Techniques

In this work Fluent (Version 6.2.16), a commercial computational fluid dynamics (CFD) software, is used to solve governing equations mentioned above, for not only the gas phase but also the dispersed phase in the cold spray process. The variables of the gas flow, such as the velocity, temperature, and pressure, are calculated by Fluent with a finite volume method. The computational domain is divided into multi-blocks and a number of quadrilateral control volumes. All the variables are solved in the center of the control volume (cell-centered arrangement). The Reynolds stress turbulence model is selected to simulate the supersonic turbulent flow.

Particles are tracked by using a two-way coupling model between the gas and particle phase. The particle velocity in a two dimension (2-D) problem has two components. One is axial-velocity, which is in the same direction of jet centreline; the other one is lateral-velocity, which is perpendicular to axial-velocity. However, the direction of the normal particle velocity upon impact may be different from that of either axial-velocity or lateral-velocity, especially for concave and convex substrate.

26

In order to consider the effect of particle dispersion and substrate shape, particle normal velocity upon impacting on the substrate is calculated based on the particle axial-velocity and lateral-velocity as well as the substrate curvature.

Normal Velocity

Figure 2-1 shows particle normal velocity upon impact on a concave substrate. The normal velocity on a concave substrate can be obtained from equation (2.17).

$$U_{normal} = U_{particle} \times Cos(\theta_1 - \theta_2) \tag{2.17}$$

where θ_1 is angle of the normal vector, θ_2 is the angle of the particle velocity, and $\theta_1 - \theta_2$ is the angle between the particle velocity and the normal vector.
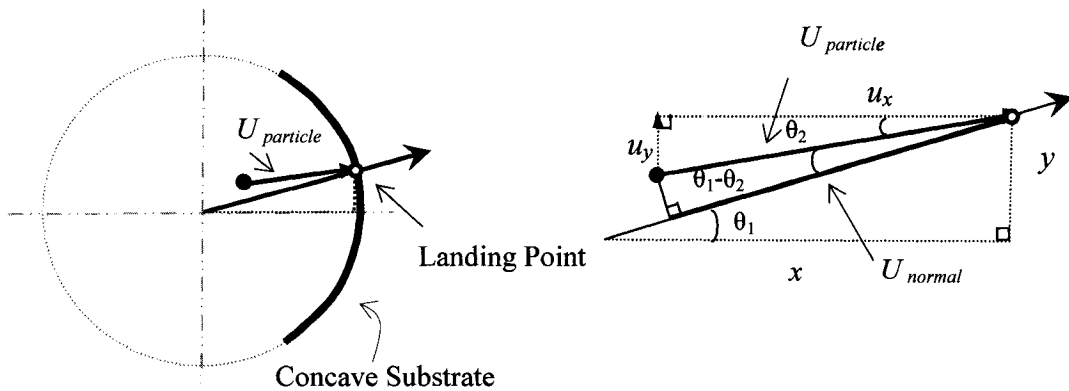
Figure 2-1 Particle normal velocity upon impact on a concave substrate

27

The normal velocity of the particle upon impact on a convex substrate can be obtained as follows (Figure 2-2).

$$U_{normal} = U_{particle} \times Cos(\theta_1 + \theta_2) \tag{2.18}$$

where $\theta_1 + \theta_2$ presents the angle between the particle velocity and the normal vector for a convex substrate.
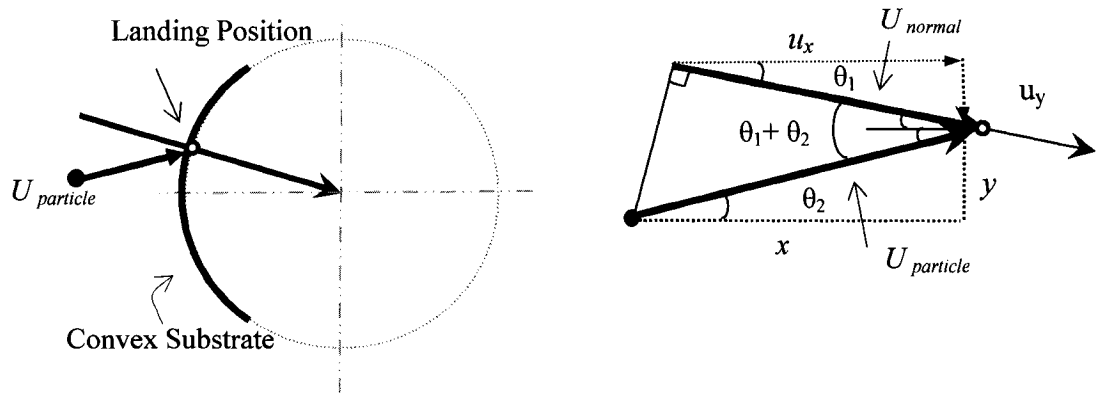
Figure 2-2   Particle normal velocity upon impact on a convex substrate

The angle of the normal vector, θ_1, and the angle of the particle velocity, θ_2, for both concave and convex substrate can be calculated by equations (2.19) and (2.20).

$$\theta_1 = arc\ tg\left(\frac{y}{x}\right) \tag{2.19}$$

$$\theta_2 = arc\ tg\left(\frac{u_y}{u_x}\right) \tag{2.20}$$

where u_y is the particle lateral-velocity and u_x denotes particle axial-velocity.

28

2.2.1. Nozzle Geometry

Figure 2-3 shows the axisymmetric nozzle geometry and dimensions. Its shape is similar to the patented nozzle of Papyrin et al. [3]. The cross-section of the nozzle is circular.
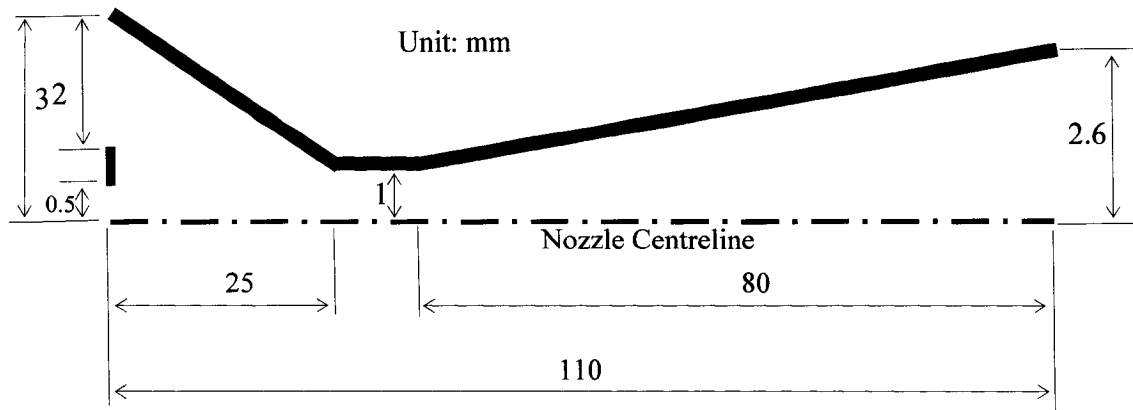
Figure 2-3   **Nozzle geometry and dimensions**

Normally, the nozzle used in the cold spray has a diverging section which is much longer than the converging section (Figure 2-3). This long diverging section can facilitate the particles to be accelerated more sufficiently inside the nozzle. However, the friction effects will increase in a longer nozzle. The proper design of a nozzle has to take both factors into consideration.

The throat areas of the nozzles used in a cold spray process are normally small in order to decrease the flow rate of the feeding gas. A large nozzle is not economical, especially in the case of using the expensive carrier gases, such as helium and nitrogen.

29

The nozzle geometry can greatly influence the gas and particle velocity in a cold spray process. As the area ratio of the nozzle exit to the nozzle throat is fixed, the maximum Mach number that can be achieved with a specific gas is also determined. The area ratio of the nozzle exit to the nozzle throat in this thesis is 6.76. The Mach number at the exit of this nozzle for an isentropic flow can reach up to 4.3 and 3.5 for helium and air, respectively.

2.2.2 Discretization

To accurately simulate the shock and expansion waves in the cold spray process, the mesh size should be fine enough. A cell size independence test is conducted to obtain the optimum mesh size. It is found when the quadrilateral mesh size for the above geometry is less than 0.2 x 0.2 mm, the computational error due to the mesh size is less than one percent. Further decreasing the cell size did not significantly improve the accuracy, but would dramatically increase the computational time. The nozzle is divided into three blocks. There are 17 vertical nodes and 551 axial nodes inside the nozzle. The total number of the nodes in the nozzle is 9365. The computational domain outside the nozzle is composed of 154 vertical nodes and 151 axial nodes. The computed cells located between the nozzle exit and the substrate is 23254 when the substrate stand-off distance is 30 mm.

30

2.2.3 Boundary Conditions

The boundary conditions applied to simulate the gas and particle flow in the cold spray process is shown in Figure 2-4. The particles are propelled by the gas flow and injected to the nozzle near the nozzle centreline. Particle velocity at the nozzle inlet is kept at a constant value, 83 m/s. The compressed gas is introduced into the nozzle from the outside of the particle inlet. The gas pressure and temperature at the nozzle inlet are kept at 23 atm and 500 K, respectively. The gas flow rate is 5 g/s. The nozzle wall is non-slipping, which means that the gas velocity near the nozzle wall is zero. The substrate is also treated as a wall. Far field boundary conditions at atmosphere pressure and temperature (1 atm, 300K) are considered for the open areas.

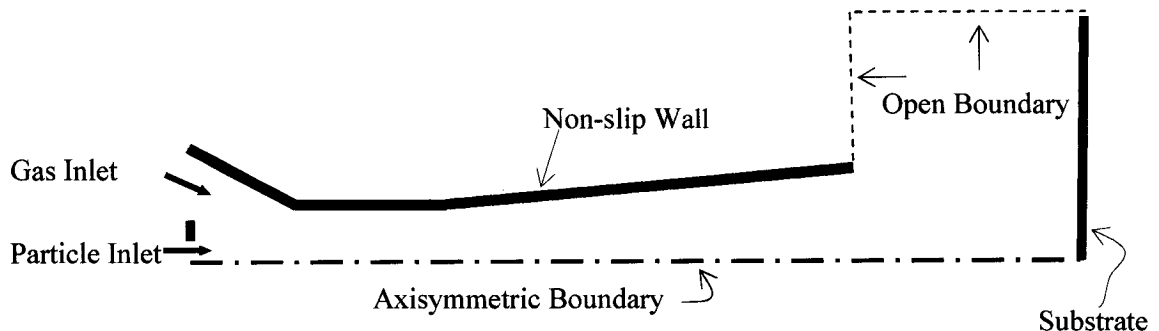Since the nozzle is axisymmetric, only half of the nozzle is needed to be modeled.

Figure 2-4   **Boundary conditions**

31

2.2.4 Carrier Gas Material and Particle Size Distribution

Carrier Gas Material

Carrier gases commonly used in cold spray processes include helium, air , and nitrogen. The criterion to choose a proper carrier gas depends on the coating material, the gas properties, and the nozzle geometry. A proper carrier gas can assure that a satisfactory particle velocity upon impact can be achieved at a reasonable cost.

Technically speaking, helium is the best carrier gas for a cold spray system. Helium is a noble gas and does not react with most metals at atmospheric condition. It can prevent the spray materials from oxidation during the coating process. Moreover, a higher particle velocity can be achieved when helium is used as the carrier gas. However, using helium makes the cold spray process extremely expensive.

Nitrogen is a general purpose gas used in the cold spray process. It is inert to most spray material while much cheaper than helium. When expanding in a nozzle, the nitrogen velocity is about one third of that of helium under the same condition.

As the cheapest feeding gas, air is also widely used in the cold spray process. The physical properties of the air are very close to those of nitrogen as the main content in the air is N_2 and O_2. The particle velocity when using air as the carrier gas is close to that of the case using nitrogen. However, air cannot be used for coating materials which can be easily oxidized, such as aluminum, copper, and some alloys.

32

Table 2-1 shows the physical properties of the three commonly used carrier gases at

25°C. The range of particle velocity in the cold spray process is compared for each case.

Gas	Molecular Mass	Gas Constant (J/Kg.K)	γ	Sound Speed at 298K (m/s)	Sound Speed at 773K (m/s)	Particle Velocity Range (m/s)
Helium	4.003	2077	1.67	1016.7	1637.4	1000-1200
Nitrogen	28.014	296.8	1.4	351.9	565.6	300-600
Air	28.967	287	1.4	346	557.3	300-600

Table 2-1 **Properties of helium, nitrogen, and air**

The equation of sound speed is:

$$a = \sqrt{\gamma R T_g} \tag{2.21}$$

where γ is C_p/C_v, R the gas constant and T_g the gas temperature.

Obviously, the sound speed of helium is much larger than that of air and nitrogen under the same operating condition because of its larger gas constant R and γ. Consequently, for the same Mach numbers, velocity of helium is much larger than that of air and nitrogen. This explains why helium is used to achieve high deposition efficiency for materials, such as ceramic and some refractory metals, which are extremely difficult to be coated by using air and nitrogen.

A commercial cold spray process has to meet a proper balance between the coating quality, deposition efficiency, and the overall cost. Therefore, the mixture of gases, such as air with helium or nitrogen with helium, can be used as feeding gas to achieve a satisfactory particle velocity.

33

Particle Size Distribution

The particles used in an actual cold spray process are normally a mixture of particles of various sizes. The percentage of each particle size, or the particle size distribution, can be obtained experimentally by using an electron microscope.

In order to simplify the calculations in our simulation, the particles of uniform size are used each time in the simulation. The simulation was repeated with uniform particles of other sizes in order to investigate the effect of particle size.

2.3. Results and Discussions

2.3.1. Gas Phase

The Mach number contours of the gas phase in a free jet are shown in Figure 2-5. Helium as the carrier gas is introduced to the de Laval nozzle. The gas flow is accelerated in the converging part of the nozzle until the Mach number reaches approximately 1 at the nozzle throat. Then, the gas develops into a supersonic flow at the diverging section of the nozzle. The Mach number of the gas flow at the nozzle exit is about 3.5. Starting from the nozzle exit, a series of shock diamonds and expansion waves are formed along the free jet. About eight shock diamonds can be identified in the free jet. Further downstream of the gas flow, the shock diamonds are dissipated and gradually die out because of the viscous effects of the turbulent flow.
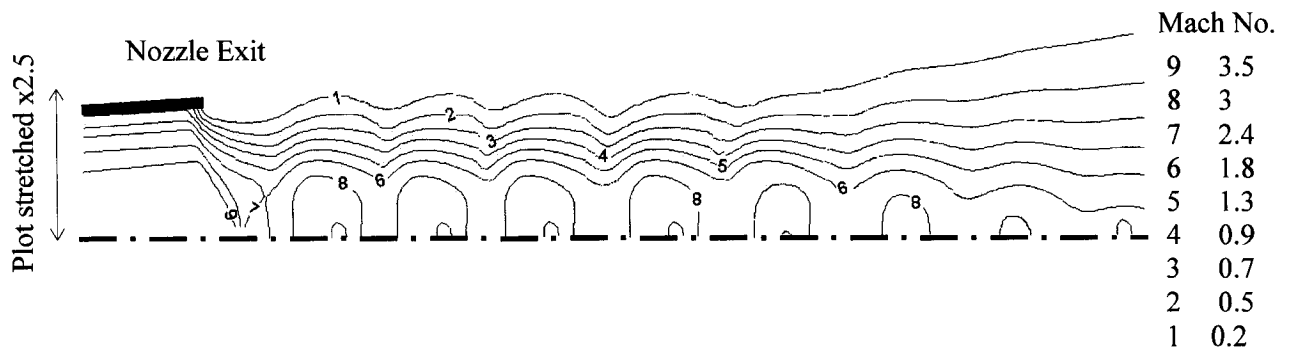
Plot stretched x2.5

Nozzle Exit

Mach No.	
9	3.5
8	3
7	2.4
6	1.8
5	1.3
4	0.9
3	0.7
2	0.5
1	0.2

Figure 2-5   Mach number contours of a free gas jet

Physics of Shock Diamonds

The physics of shock diamonds can be explained as follows:

For an over-expanded nozzle, the exit pressure at the exit plane of the nozzle is less than the atmosphere pressure. Supposing the stagnation pressure and temperature in the chamber of nozzle remain constant, the flow will adjust to the back pressure in the form of compression waves or expansion waves outside the nozzle, rather than inside the nozzle. As shown in Figure 2-6, an oblique shock wave occurs at the exit plane (A) of the nozzle to increase the pressure. The gas is compressed when passing through the oblique shock. The gas pressure increases and the gas direction is towards to the centerline (2). Since the central streamline works as a wall plane, the gas cannot pass through it, neither the oblique shock. Therefore, reflected oblique shocks are formed and reflected outward (B). This reflected shock wave now turn the gas passing through it back to parallel (3) to the centreline. However, the pressure of the exhaust gas now increases further to be above the ambient pressure.
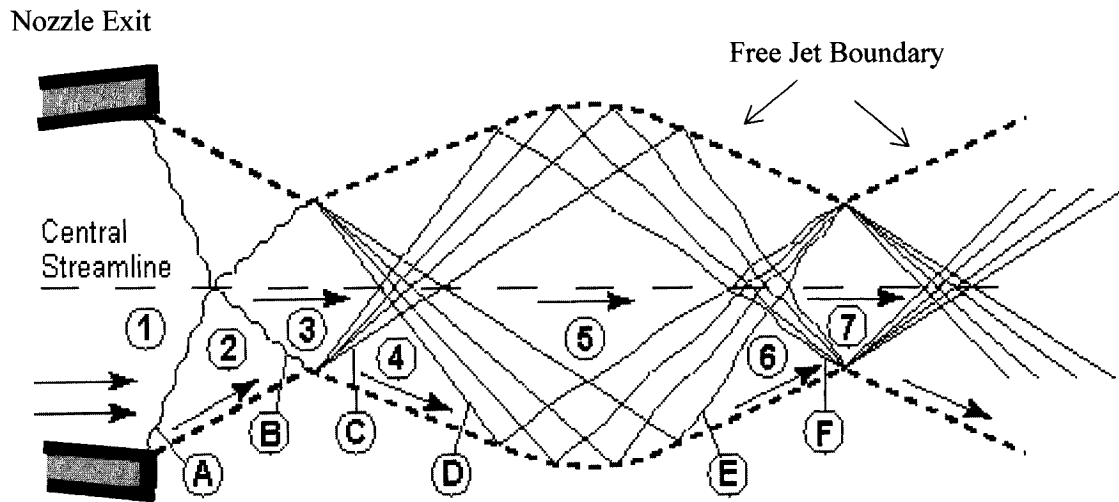
35

Figure 2-6 Physics of shock diamonds

At this time the reflected oblique shock wave reaches the boundary where the exhaust gas meets the free stream line with the same pressure inside and outside the boundary. The boundary is termed the contact discontinuity. Since the pressure of the exhaust gas is greater than the ambient air pressure, the reflected oblique shock now turns back to the centreline from the boundary (C) in the form of Prandtl-Meyer expansion Mach wave(C). When the gas passes through the expansion fan, its pressure is decreased and the gas direction now turns outward of the centerline (4). To make the gas flow straightforward, when the Prandtl-Meyer expansion waves hits the centre plane, it is reflected to the contact discontinuity (D). The reflected expansion wave reduces the exhaust gas pressure passing through and straightens the gas to be parallel to the centreline.

36

At this time the gas pressure is below the ambient air pressure. To increase the pressure, Prandtl-Meyer compression waves (E) yield when the expansion waves reflect from the contact discontinuity. When the exhaust gas passes through the compression wave, the gas pressure is increased to the ambient pressure. On the other hand, the gas direction is back towards the centreline (6). The further reflected compression waves turn the flow parallel to the nozzle centerline and increase the gas pressure above ambient(7). Now the situation is similar to that of (B) when it went through the reflected shock wave with high pressure and straightforward direction (3). The shape of this interaction by the expansion and compression waves looks like a diamond. The gas will continue to expand and compress in the same way until the pressure is equal to the ambient pressure and the flow is parallel to the nozzle centreline. These repeated cycles produce a diamond shape chain that dies out by viscous effect from the ambient air along the jet boundary.

The gas Mach number contours near the flat, concave, and convex substrates are also shown in Figure 2-7 in which all the substrates are located at 20 mm from the nozzle exit. Two shock diamonds are formed between the nozzle exit and the substrate. Compared to that observed in a free gas jet, the number of shock diamonds is decreased because of the presence of the substrate. A strong bow shock is formed near each substrate (flat, concave, and convex substrate) when the supersonic flow impinges on the substrates. Finally, the gas flow turns to different directions according to the curvature of the substrate. Clearly, the motion of the particles will be dramatically affected by the gas flows near the flat, concave, and convex substrates.
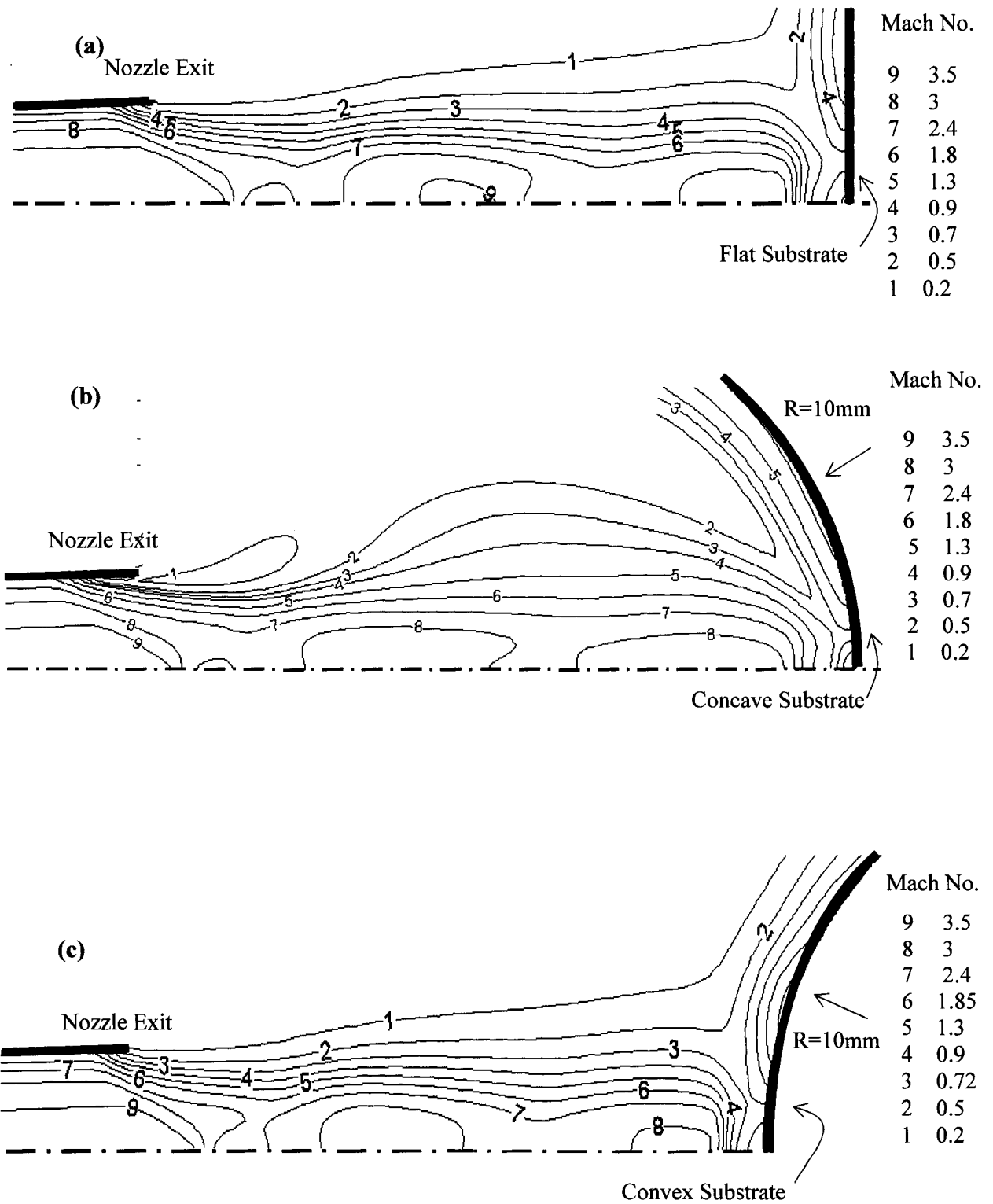
Figure 2-7   Gas Mach number contours near (a) flat, (b) concave, and (c) convex substrates

38

2.3.2. Particle Phase

2.3.2.1 Effect of Shock Diamond and Bow Shock

The effect of the shock diamonds and the bow shock on the particle velocity is shown in Figure 2-8. This demonstrates how the particle velocity changes along the jet after it passes through the shock diamonds and the bow shock. Starting from the nozzle exit to the substrate, the velocities of one thousand copper particles (particle size: 20 μm) are calculated using two different drag coefficient correlations; Igra and Takayama [26] as well as Henderson [27]. As it is demonstrated in Figure 2-8, at the nozzle exit, the axial particle velocity for both correlations is close to each other (about 1800 m/s). The mean particle axial velocity using the two models decreases gradually between the nozzle exit and the bow shock. This is because the kinetic energy of the gas flow also dissipates gradually in the turbulent flow after it passes through the shock diamonds. A sharp reduction in the particle velocity is observed in the area near the flat substrate where a strong bow shock is formed. After entering the bow shock, the mean particle velocity calculated by Henderson's correlation decreases from 1600 to 349 m/s, while the mean particle velocity calculated by Igra and Takayama's model changes from 1600 to 492 m/s.

Particle normal velocity decreases noticeably near the substrate, not only because of the bow shock, but also because of the existence of a stagnation core area between the bow shock and the substrate. The shape of the bow shock and the stagnation area can be clearly identified in Figure 2-9, where the stand-off distance of the substrate is 10 mm. It can be seen that in the area that the bow shock is formed, the trajectories of 1 μm copper

39

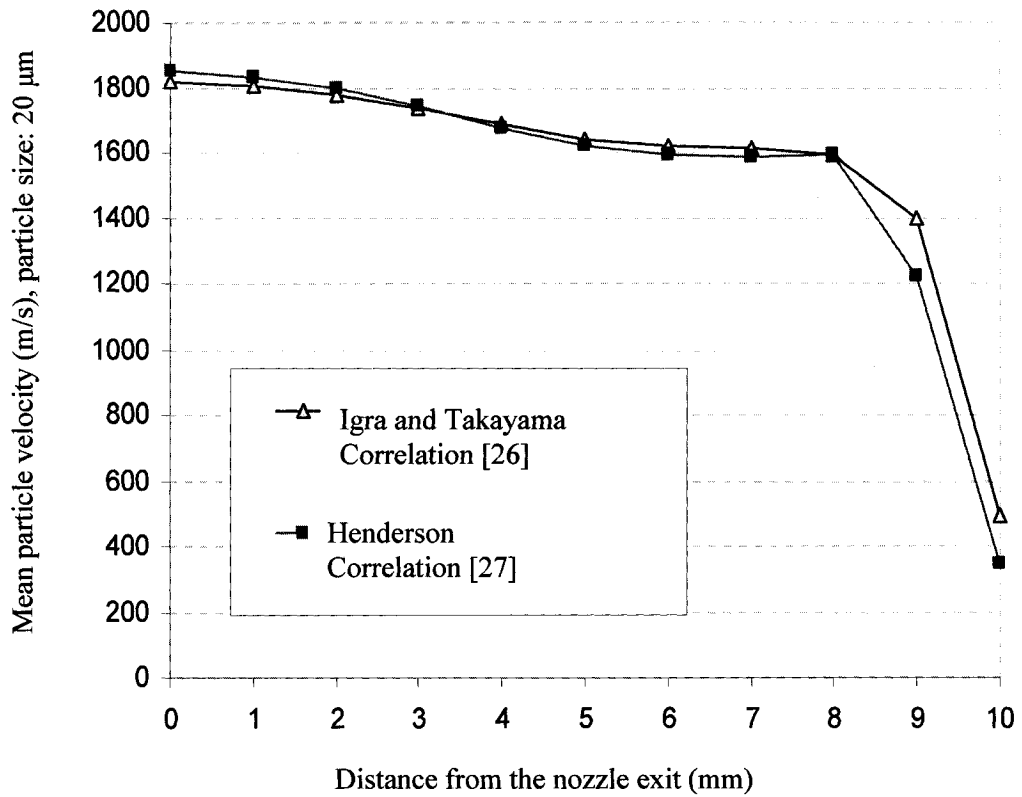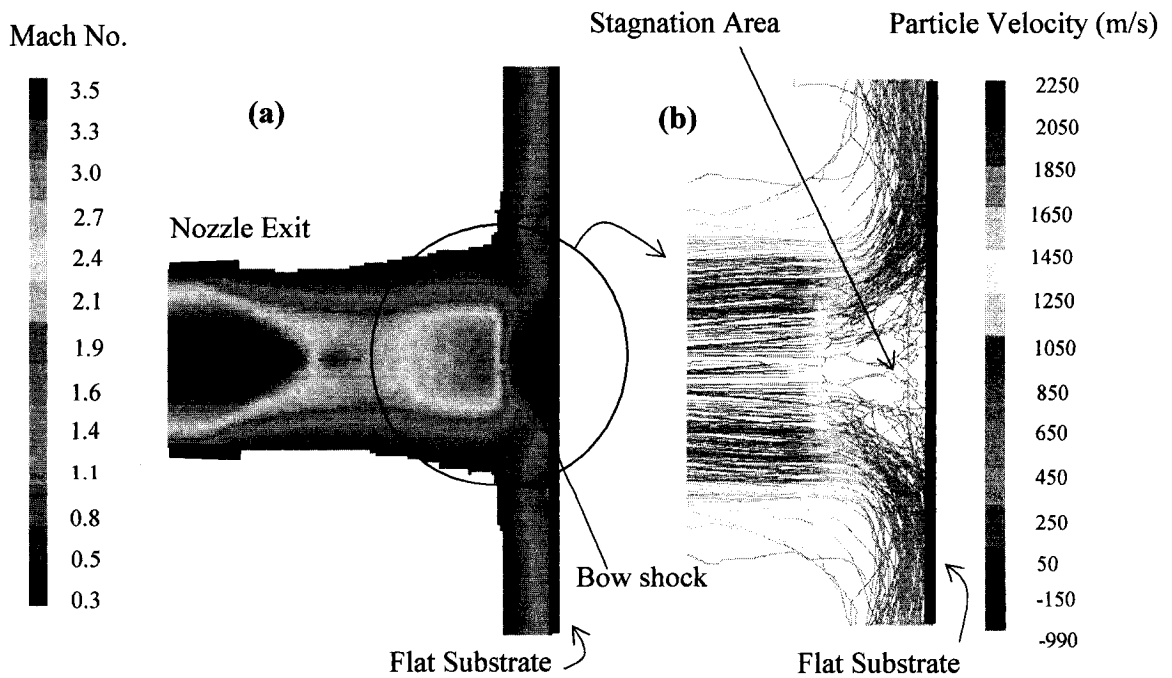**Figure 2-8   Effect of shock diamonds and bow shock on mean particle velocity**

Figure 2-9   **Gas and particle flow near the substrate placed at a stand-off distance of 10 mm:**

(a) Mach number contours, (b) particle trajectories

40

particles are deflected and the particles go away from the centreline. The high pressure in the stagnation area also turns the particles away from the axial direction. Combination of the two effects dramatically decreases the magnitude of the normal velocity.

In this thesis Henderson's correlation is utilized to predict the optimum substrate location (i.e. optimum stand-off distance), while Igra and Takayama's correlation is employed to estimate the optimum particle size and the effect of the substrate geometry.

2.3.2.2 Effect of Substrate Location

The effect of substrate location is analyzed by calculating the mean particle normal velocity upon impact for various stand-off distances ranging from 5 to 50 mm. As shown in Figure 2-10, when the substrate is located at 5 mm from the nozzle exit, the calculated mean particle velocity is about 240 m/s which is rather low. This is because of the formation of a strong bow shock when the substrate is located very close to the nozzle exit. This strong bow shock results in negative effect on the mean normal velocities of the particles. On the other hand, when the stand-off distance is 50 mm, the calculated mean normal velocity is about 280 m/s which is also relatively small. This is due to the result of strong decay in kinetic energy of both gas and particles in the viscous turbulent flow. The optimum substrate location is observed at a stand-off distance of 11 mm, where the bow shock is not so strong and the kinetic energy of the particles is relatively high.
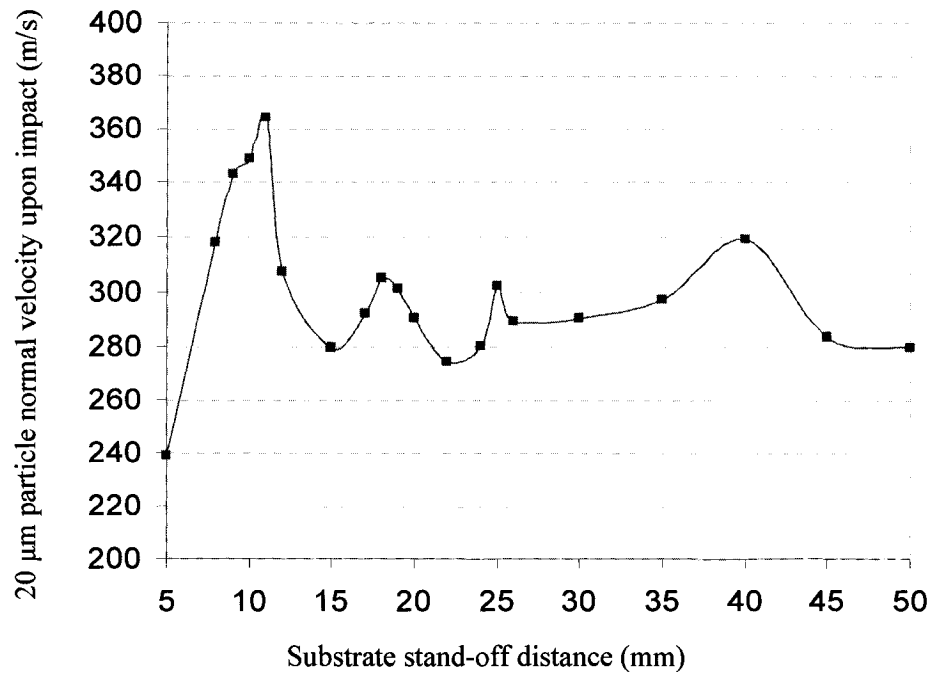
41

Figure 2-10   Effect of substrate stand-off distance on mean particle velocity upon impact
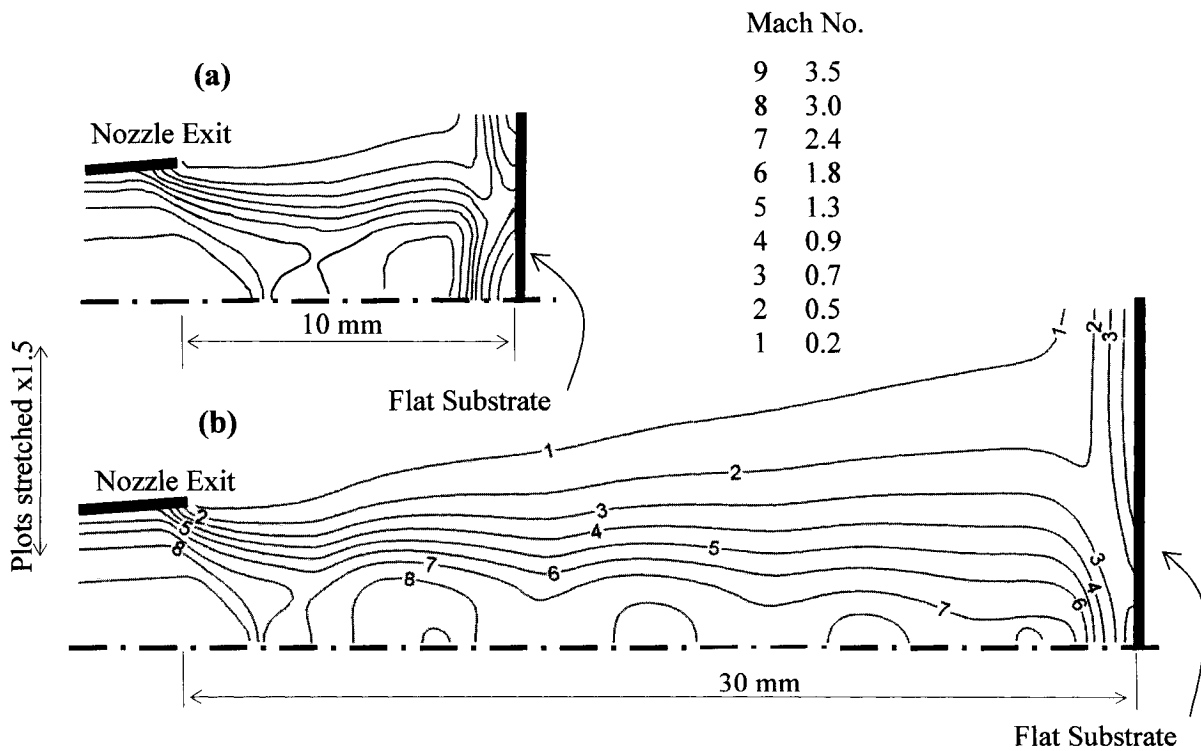

Figure 2-11   Interaction of shock diamonds and bow shock for substrate stand-off distance of (a) 10 mm, (b) 30 mm

42

There are three other local maximum velocities at stand-off distances of 18, 25, and 40 mm. These local maxima are caused by the totalized effects of the bow shock, the dissipation and the shock diamonds which alternates for the different stand-off distances. As the substrate stand-off distance is increased from 5 to 50 mm, the strength of the bow shock near the substrate would decrease accordingly, resulting in lower negative effect on the particle velocity. However, the kinetic energies of both the gas and particle phase dissipate more if the stand-off distance is increased, which may have a higher negative effect on the particle velocity. At the same time, more shock diamonds are generated between the nozzle exit and the substrate if the substrate is located further away from the nozzle exit. As shown in Figure 2-11, only one shock diamond is formed when the substrate stand-off distance is 10 mm. As the stand-off distance is increased to 30 mm, up to four shock diamonds are generated between the nozzle exit and the substrate. The particle velocity is found increasing in the shock areas, while decreasing in the subsonic areas locating between the shocks. The interaction between bow shock and shock diamonds, as well as the total amount of energy dissipation result in those maxima values at stand-off distances of 18, 25, and 40 mm.

2.3.2.3. Effect of Particle Size

Size of a particle can significantly affect its velocity upon impacting on a substrate in a cold spray process. The goal in this section is to determine the optimum particle size which results in the largest mean particle normal velocity upon impact. This will allows us to improve the coating deposition efficiency and quality. The correlation of Igra and Takayama [26] is used as the drag law. Helium and nitrogen are used separately as the

43

carrier gas in order to compare the mean particle normal velocity[*]. In both cases, when using small copper particles, for example, particles with a size of 10 μm or less as shown in Figure 2-12 (a), the mean normal velocity upon impact is low because the dispersion effect of the small particles is very strong. This negatively alters the direction of the particle velocity and causes an off-normal impact at the landing point. Particle deviation from the centreline (or dispersion effect) will be reduced for larger particles. For instance, the trajectories and velocity distribution of 45 μm particles are illustrated in Figure 2-12 (b). It is clear that particles with sizes larger than 45 μm remain close to the centerline and are less affected by the local variations of the flow field. On the other hand, large particles are difficult to be accelerated to high velocities due to their high Stokes number, which is the ratio of the particle momentum response time to the time characteristic of the fluid flow.

In order to find the optimum particle size for the given operating conditions, particles with sizes 10, 15, 20, 25, 30, 35, 40, and 45 μm are injected to the nozzle and mean particle normal velocity upon impact are numerically calculated (Figure 2-13). Interestingly, for both cases using helium and nitrogen as the carrier gas the optimum particle size is found to be about 35 μm. In Figure 2-13 it can also be observed that when using nitrogen (or air) as the carrier gas, the mean particle normal velocity upon impact is lower than that of the case using helium. For practical applications, to obtain a satisfactory normal velocity, a mixture gases of nitrogen and helium, can be used to regulate the particle velocity.

---

[*] It is important to mention that similar numerical simulations have been carried out using air as the carrier gas and the results were very similar to that of the case using nitrogen.
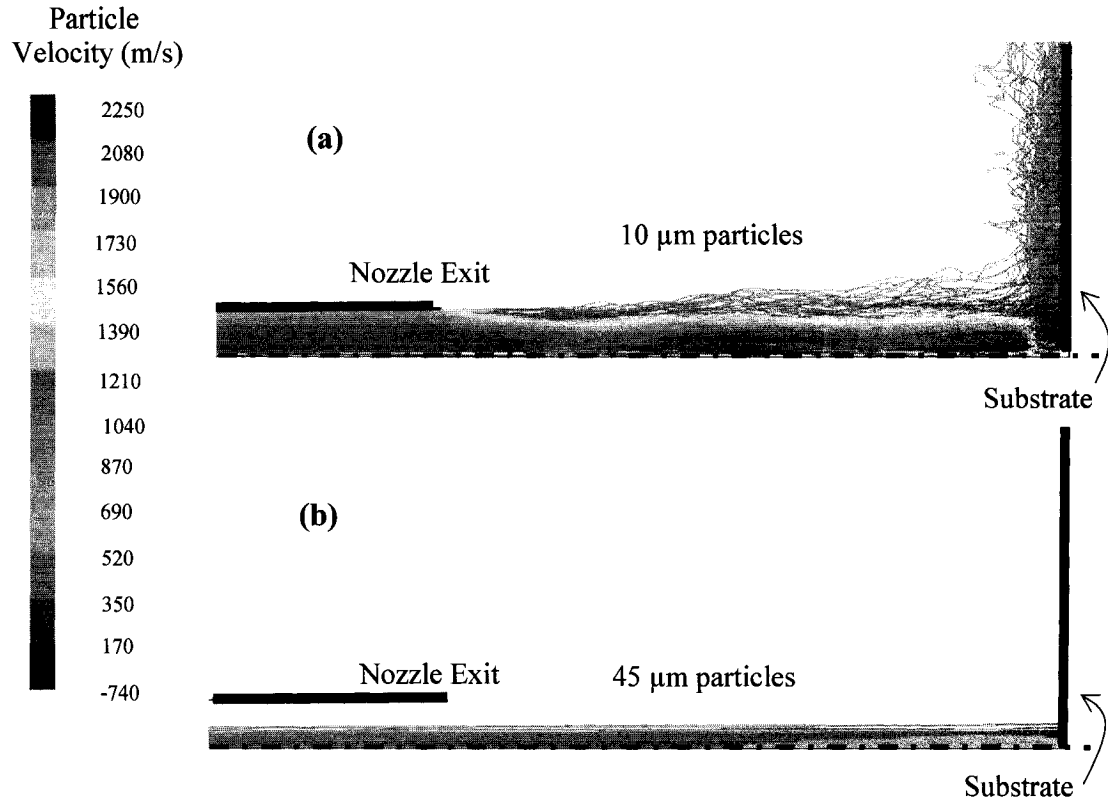
44

Figure 2-12   Trajectories and velocity distribution of (a) 10 μm and (b) 45 μm copper particles
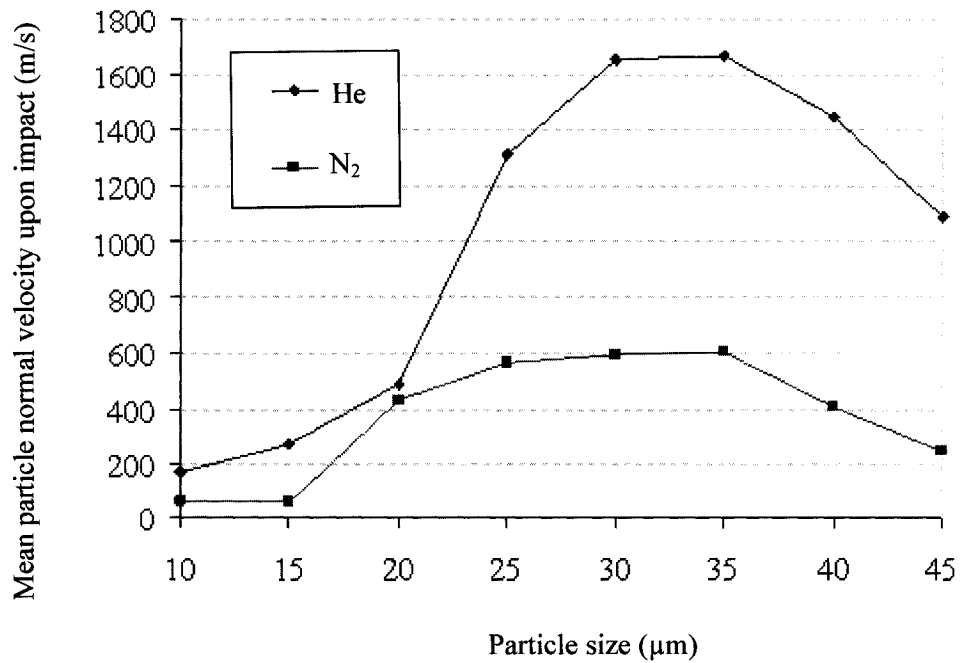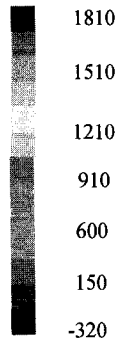

Figure 2-13   Optimum particle size

45

2.3.2.4. Effect of Substrate Geometry

Substrate geometry has a complex effect on the overall flow field and particle deposition because it alters not only the normal direction of the particle landing points, but also the gas flow and the particle velocity. As an example, Figure 2-14 shows trajectories and velocity distribution of 20 μm particles near three different substrates; flat, concave, and convex. The normal particle velocity upon impact would be significantly affected by the substrate curvature as well as the bow shock formed on the substrate. Combination of the two effects results in completely different particle trajectories and velocity distribution for the three substrate geometries.

The effect of the substrate geometry on the mean normal velocity also depends on the particle size. As it is demonstrated in Figure 2-15 for particles with a size of 25 μm, the mean normal velocity upon impact on the convex substrate is 978 m/s, which is 20% more that that of the cases with flat and concave substrates. This is due to the weaker bow shock associated with a convex substrate as it compares with the flat and concave cases. However, for particles larger than 35 mm, the calculated mean normal velocities upon impact on the flat, concave, and convex substrates are close to each other because large particles are less sensitive to the bow shock. It is also shown that the deposition of small particles on a concave substrate turns to be the most challenging task because of the strong bow shock and the backward gas flow near the concave substrate. Most of the small particles escape from a concave substrate without deposition.

46

Particle Velocity (m/s)

1810
1510
1210
910
600
150
-320

(a)

Nozzle Exit

Flat Substrate

Particle Velocity (m/s)

1810
1660
1080
560
40
-490
-1020

(b)

Nozzle Exit

R=10 mm

Concave Substrate

Particle Velocity (m/s)

1810
1510
1210
910
150
600
-320

(c)

Nozzle Exit

R=10 mm
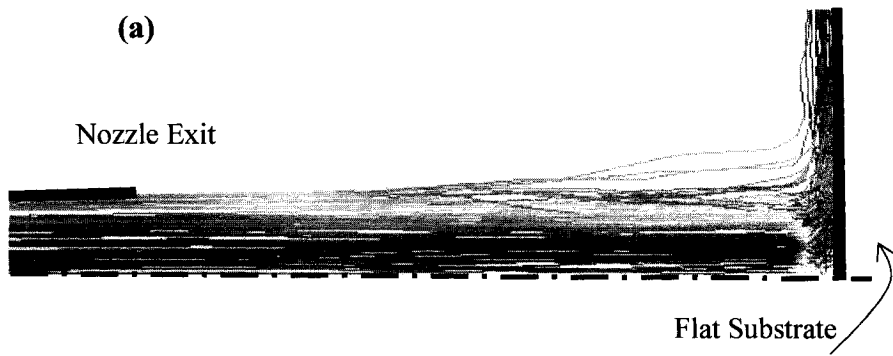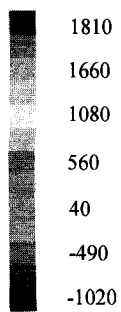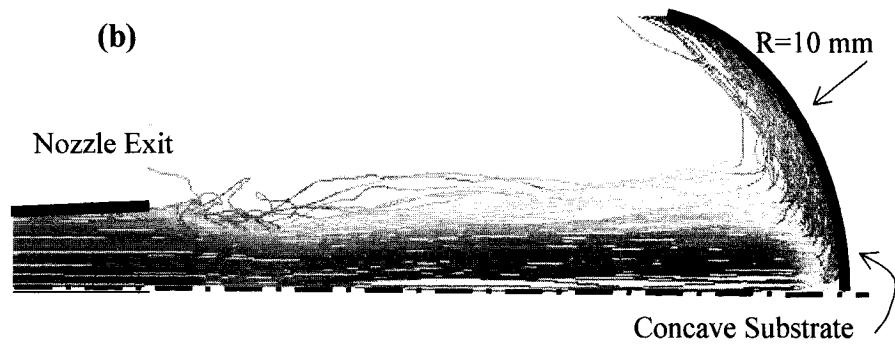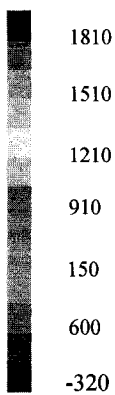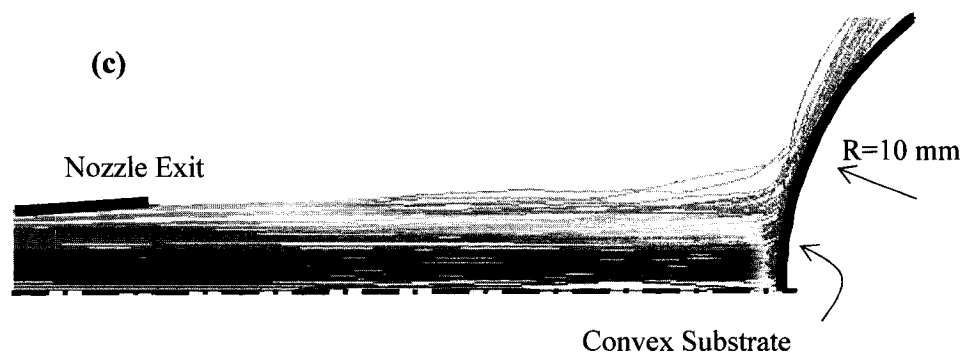
Convex Substrate

Figure 2-14   Particle (20 µm) trajectories near a (a) flat, (b) concave, (c) convex substrate

47
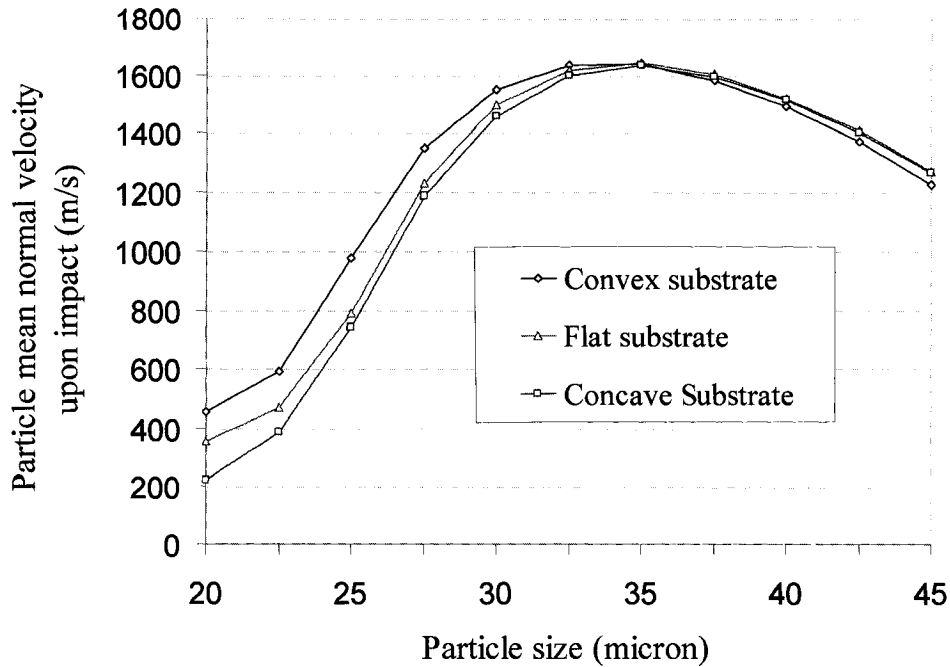
Figure 2-15 Effect of substrate geometry on mean particle velocity upon impact

2.4. Experimental Validation

The results and conclusions mentioned above are based on the calculation of particle normal velocity upon impact. These results have not been validated because the normal velocity of the particle upon impact is very difficult to be measured experimentally. One reason is that particle motions are very irregular near the substrate. In a specific small measuring volume near the substrate, particles can be moving forward or be bouncing back from the substrate, or deviating from the jet centreline because of the bow shock and the gas turbulence. Another reason is that the velocity sensors, such as a Laser Doppler Velocity (LDV) or an in-flight particle diagnostic system (DPV-2000), cannot measure the particle velocity upon impact because of the existence of the substrate.

48

As a result, the particle velocity measured in a free jet is usually used to validate the simulation results.
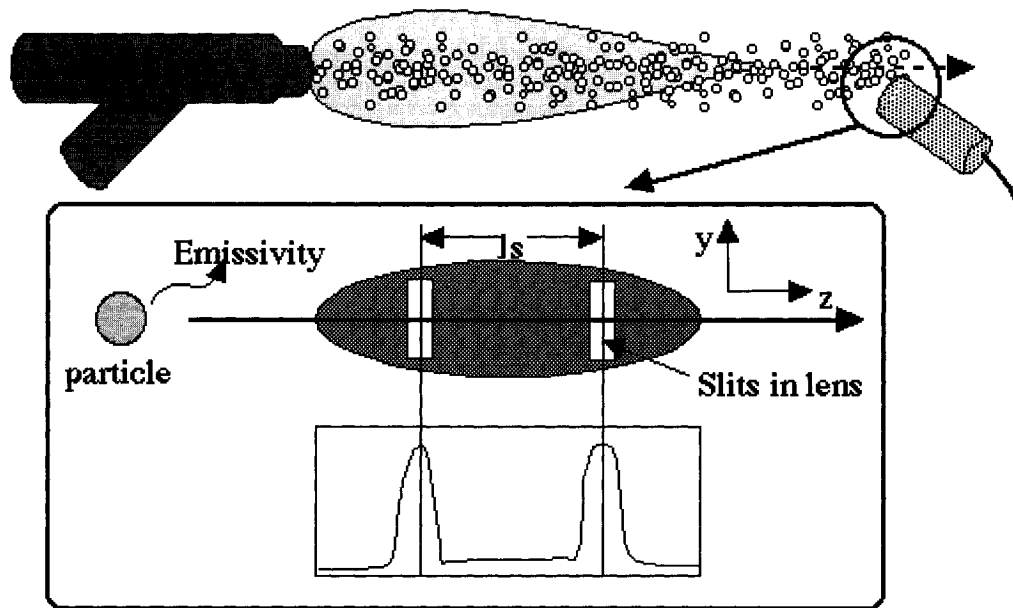
Figure 2-16   DPV 2000 sensor head and particle detection mechanism

In this thesis, some joint works have been conducted through collaboration with National Research Council Canada (NRC-IMI, Boucherville, Quebec) in order to verify the accuracy of the simulation results. Experiments were conducted at NRC-IMI with a Supersonic Spray Technology (SST) cold spray system from Centerline Limited (Windsor, Ontario). Particle velocity is measured in the experiment of NRC-IMI by a DPV-2000 [28] system from Tecnar Inc (St. Bruno, Quebec). DPV-2000 is an in flight particle sensor for thermal spraying systems (Figure 2-16). As a high speed, high precision two colour optical sensing device, DPV-2000 can monitor on-line the particle velocity, temperature and size. Finally, the experimental results obtained from DPV-2000 were compared with the simulation results. The simulation was carried out with the same

49

nozzle geometry as that used in the experiments conducted at NRC-IMI. The dimensions of the nozzle are shown in Figure 2-17. The cross-section of the nozzle is circular. The radius of nozzle inlet, throat, and exit are 4, 2, and 3 mm, respectively. The length of nozzle diverging section is 97 mm, which is much longer than the converging section (25 mm). The total length of this nozzle is 157 mm. The area ratio of the nozzle exit to throat is 2.25. The gas Mach number of this nozzle can reach up to 2.5 in an isentropic flow.
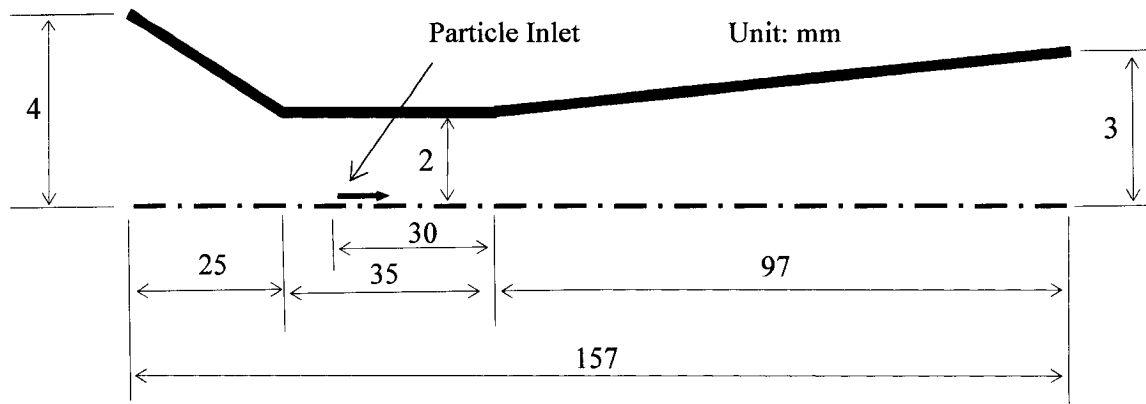
Figure 2-17   Simplified nozzle geometry used by NRC-IMI

The mesh size of this nozzle is about 0.2 x 0.2 mm. When the substrate is kept at 30 mm away from the nozzle exit, the whole computational domain consists of 13362 cells.

Air is used as the carrier gas. The flow rate of the air is 12.37 g/s. The pressure of air at the nozzle inlet is kept at 90 psi. The air is preheated to 500 °C before it is input to the nozzle inlet.

Aluminum particles are used as the coating material. In the experiment, the particles are sucked into the nozzle from a hole on the nozzle wall where the pressure of the gas flow is below the atmospheric pressure. Since particles are not axisymmetrically injected into the nozzle, a 3-D model would be preferable to simulate this process. However, to

50

simplify the simulations, particles are injected into the nozzle near the nozzle centreline, at a location which is 30 mm away from the nozzle inlet. Consequently, this problem is changed to an axisymmetric 2-D problem by changing the way of particle injection. Since particles are mainly accelerated by the gas flow in the diverging section of the nozzle, the error resulted to the particle velocity from this simplification can be neglected. Particles are injected with a velocity of 25 m/s and a temperature of 500 °C.

The aluminum powder used in the experiments by NRC-IMI is a mixture of particles of various sizes. The mean and the median particle size of this mixture are 36.2 and 33.3 μm, respectively. The particle size distribution is illustrated in Figure 2-18. A user-defined particle-injection data file which produces the same particle size distribution mentioned above was employed and hooked to the Fluent code. The Reynolds stress turbulence model was used to simulate the turbulent supersonic flow.
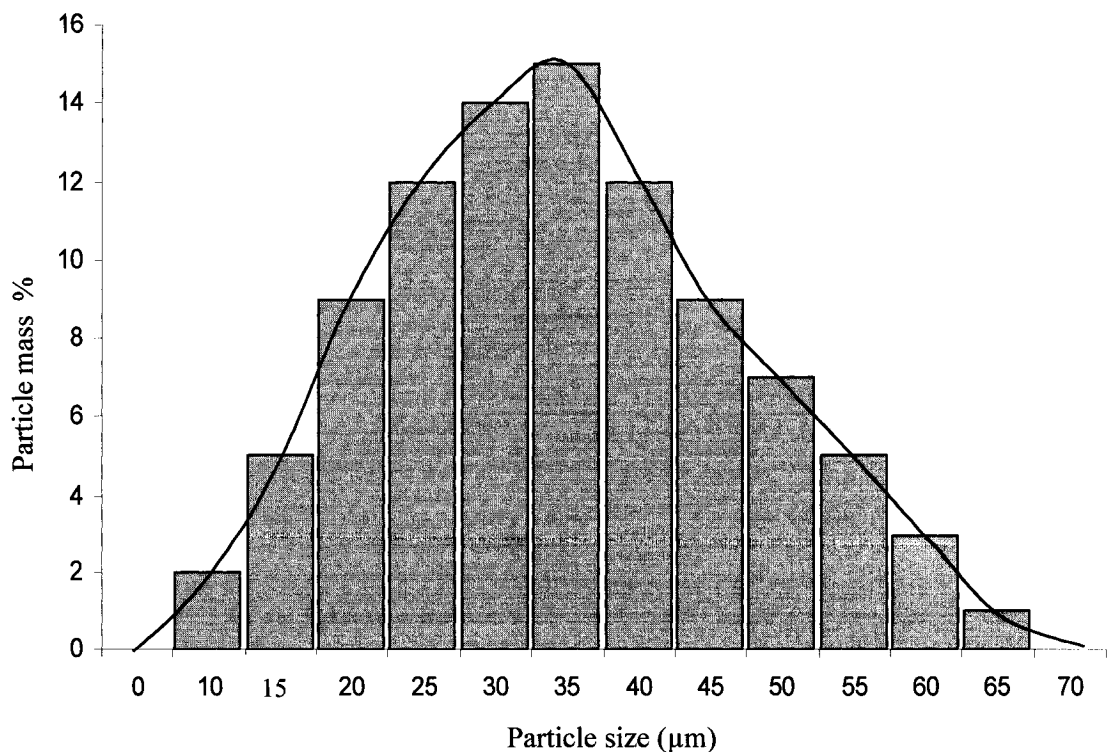
Figure 2-18   Particle size distribution provided by NRC-IMI

51

The Mach number contours of the gas phase are shown in Figure 2-19. At the

nozzle exit, the Mach number is about 2.3. Three shock diamonds are produced in the

free jet outside the nozzle. Particles with the given size distribution are tracked in the free

jet at a cross-section of the flow at 10 mm far away from the nozzle exit, just as that in

the experiment.
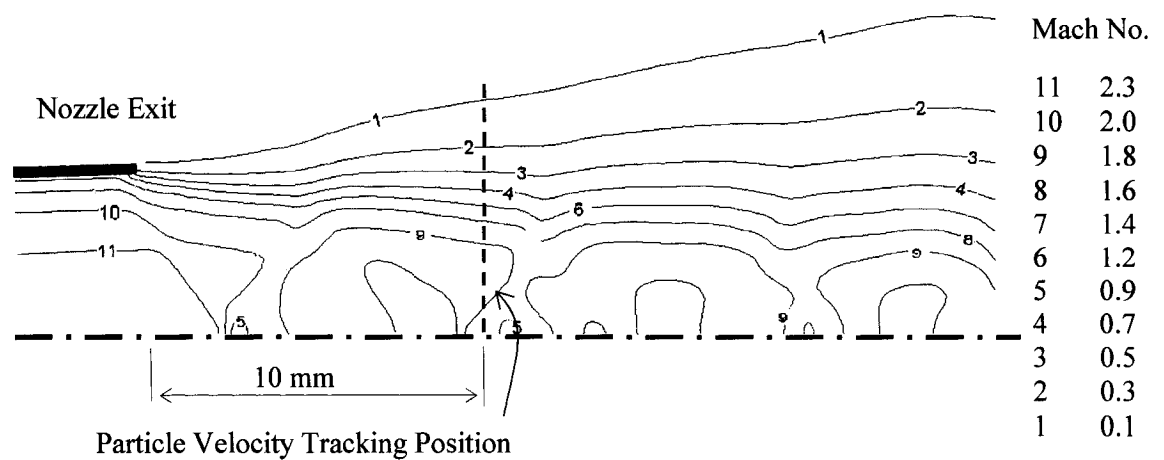
Figure 2-19 Mach number Contour of NRC-IMI nozzle

The velocity of one thousand particles is calculated. The mean particle velocity

obtained in the simulation is 487 m/s, which is very close to the experimental result, 486

m/s, as shown in Figure 2-20. It can be concluded that the numerical model can

accurately predict the mean particle velocity. As a result, the deposition efficiency of the

cold spray process can be evaluated based on the mean particle velocity.
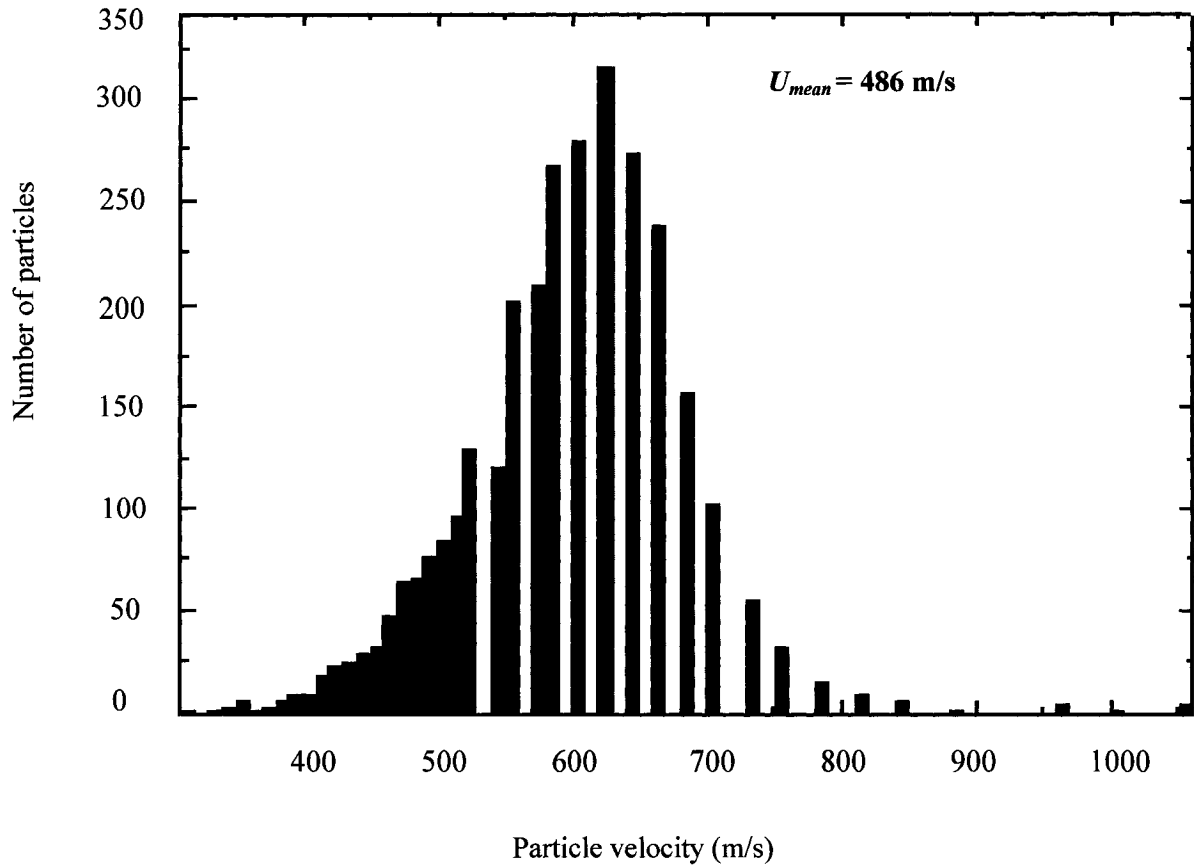
Figure 2-20 Particle velocity measured by NRC-IMI

Although the numerically calculated mean particle velocity is very close to that of

the experimental results, the simulated particle spatial distribution is different from that

of the experiment. The trajectories of the particles in the simulation are concentrated to a

small circular area near the jet centreline (Figure 2-21). However, the experimental

results show that the particles are dispersed more than 3 mm away from the jet centreline

at the measuring position (Figure 2-22). The deviation from the centreline is more

pronounced for particles with sizes less than 20 μm. The difference in the particle spatial

distribution between the numerical and experimental results can be due to the 2-D

axisymmetric assumption made in the numerical simulation. In practice, particles are

injected from the nozzle wall at an angle of approximately 45°. Therefore, particle initial

53

velocity is not in the same direction as that of the gas flow. As a result, the particles injected from the nozzle wall would disperse further away from the jet centreline, compared to those injected from the nozzle centreline. The dispersion of the small particles is larger than that of the larger particles because the Stokes number associated with small particles is very small. In addition, larger particles are found moving below the nozzle centreline at the measuring point. When the larger particles are injected from the nozzle wall, they pass through the nozzle centreline because they are less sensitive to the gas flow. This is why the large particles are located below the nozzle centreline at the measuring area shown in Figure 2-22.

Particle Velocity (m/s)

730

670

600

550

490

440

380

320

260

Nozzle exit
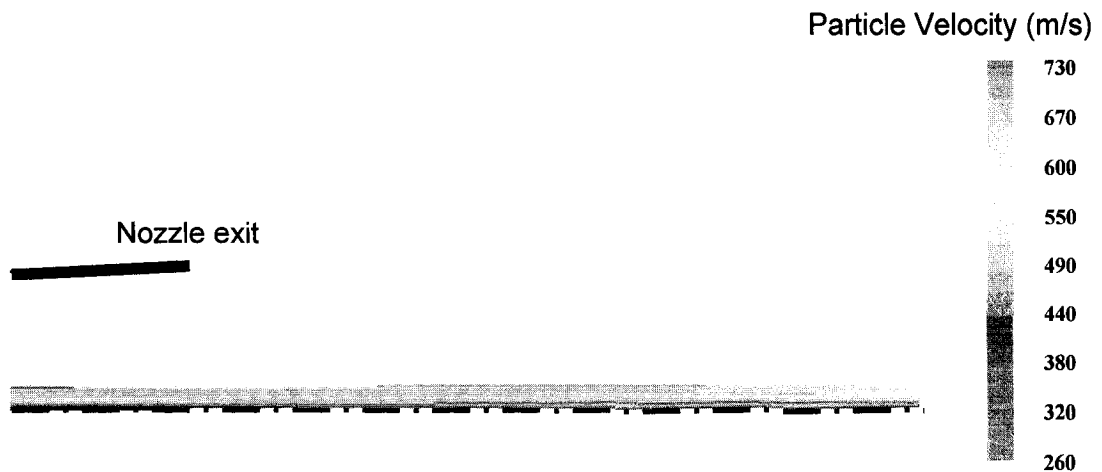
Figure 2-21 Simulated particle trajectories

54
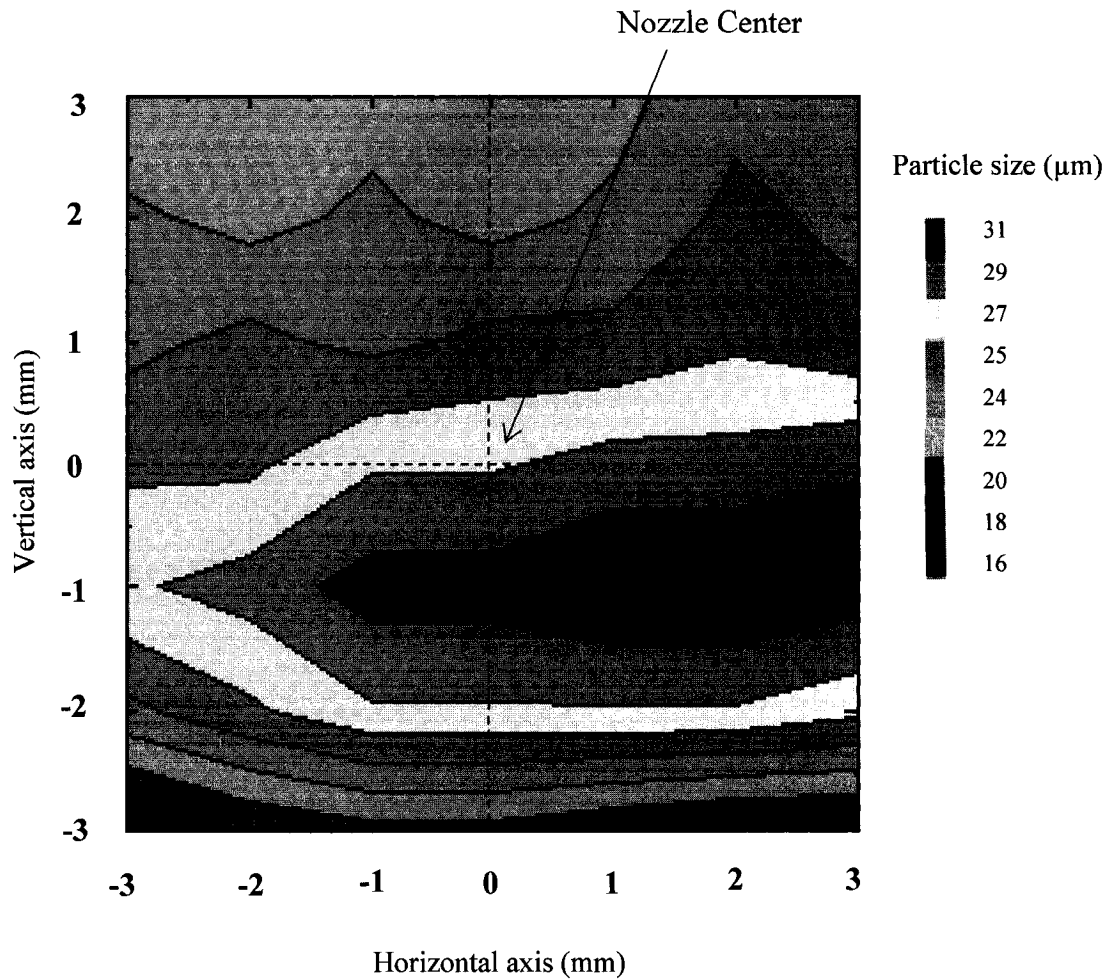
Figure 2-22   Experimental results on particle spatial distribution at a stand-off distance of 10 mm (provided by NRC-IMI)

In order to investigate the relationship between the mean particle velocity and the process parameters, more simulations have been carried out with various inlet gas pressures and temperatures. It is found that the mean particle velocity increases when the carrier gas is preheated to higher temperatures. As presented in Table 2-2, under the same pressure (90 psi), when the gas temperature is increased from 33 to 500 °C, the mean particle velocity will increase from 357 to 487 m/s. This clearly shows that one can benefit significantly by increasing the temperature of the carrier gas to improve the

55

deposition efficiency. Furthermore, the gas pressure is also found to be an important factor affecting the mean particle velocity. Decreasing the gas pressure from 90 to 50 psi will result in lowering the mean particle velocity from 487 to 439 m/s.

Process Parameters (Gas)		Simulation Results of Aluminum Particles	
Inlet Pressure (psi)	Inlet Temperature (°C)	Mean Velocity (m/s)	Std. Div. (m/s)
90	33	357	39
90	200	415	52
90	400	466	64
90	500	487	70
70	500	468	69
50	500	439	66

Table 2-2   Relations between mean particle velocity and process parameters

56

3. Eulerian Approach

In a dense flow where particle-particle and particle-gas interaction effects cannot be neglected, the Eulerian-Eulerian approach [10 and 11] because of accounting the volume fraction of the dispersed phase, will be a natural choice compared to the Eulerian-Lagrangian approach [8 and 9] to capture physical characteristics of the two-phase flow. Treating both gas and particulates as continuum phase is called two-fluid approach or simply Eulerian method. In the Eulerian approach cloud of particles passes through fixed control volumes, which are fine cells of the computational domain. Particle conditions are calculated by solving the governing equations, such as the equation of conservation of mass, momentum, and energy for both phases.

The numerical technique used in the present work is the Implicit Continuous-fluid Eulerian (ICE) method [29, 30, and 31]. ICE is a finite volume method based solver for compressible and multiphase flow. The principal variables, referring to the species mass, momentum, and energy are located at the cell-center. The flux of mass, momentum, and energy are calculated across each face of the cell to satisfy the conservation of mass, momentum, and energy within each computational cell.

57

3.1. Methodology

3.1.1. Governing Equations

The governing equations are the conservation of mass, momentum, and energy equations [31].

Conservation of mass

$$\frac{\partial \rho_m}{\partial t} + \nabla.\rho_m \vec{U}_m = 0 \tag{3.1}$$

Conservation of momentum

$$\frac{\partial \rho_m \vec{U}_m}{\partial t} + \nabla.\rho_m \vec{U}_m \vec{U}_m = -\theta_m \nabla p - \nabla \theta_m \left(p_m^o - p\right) - \nabla.\left(\alpha_m \rho_o \vec{U}'_m \vec{U}'_m\right)$$
$$+ \nabla.\left(\alpha_m \tau_o\right) + \rho_m \vec{g} + \sum_l \theta_m \theta_l K_{m,l}\left(\vec{U}_l - \vec{U}_m\right) \tag{3.2}$$

Conservation of energy

$$\frac{\partial \rho_m e_m}{\partial t} + \nabla.\rho_m e_m \vec{U}_m = -p_m \nabla.\vec{U}^f + \alpha_m \gamma_o^{-1}\left(p_o - p\right) - \nabla.\left(\alpha_m \rho_o e_o \vec{U}'_m\right)$$
$$+ \frac{\alpha_m \tau_o : \varepsilon_o}{2} - \nabla.\alpha_m q_o + \sum_l \theta_m \theta_l R_{m,l}\left(T_l - T_m\right) \tag{3.3}$$

where $\vec{U}$ denotes the velocity vector, ρ the density, p the pressure, e the internal energy, T the temperature, τ_o the stress tensor, K and R the momentum and heat exchange coefficients between phases, α the volume fraction and θ_m its expected value for material m. Since the species in the cold spray process are non-reactive, θ_m can be expressed as follows:

$$\sum_m \theta_m = 1 \tag{3.4}$$

58

There are seven unknown variables in the above 5 equations. To close the equation system, the equation of states is also needed to be solved.

$$p = (\gamma - 1)\rho e \qquad \text{and} \qquad T = \frac{(\gamma - 1)}{R}e \qquad (3.5)$$

where R, γ, and ρ represent the gas constant, specific heat ratio (C_p/C_v), and density, respectively.

The exchange terms for mass, momentum, and internal energy among species are zero because the cold spray flow is non-reactive. Some assumptions in the integration and discretization of the governing equations are made to simplify the calculation for the compressible multi-material flow.

- The non-equilibrium pressure term and the multiphase Reynolds stress are neglected.

- The feeding gas is assumed to be a perfect gas.

- The ratio of specific heats, γ, is constant.

- A first-order finite difference scheme is used for the time derivatives.

3.1.2. Algorithm Description

The computational domain in the present work is composed of a number of quadrilateral control volumes. A typical grid arrangement is shown in Figure 3-1. The indices for x, y, and z direction are i, j, and k, respectively. In addition, the face of interest is shown by the fourth index. Cell faces left, right, bottom, top, back, and front are denoted by L, R, B, T, BK, FR, respectively. Furthermore, each computational domain is surrounded by two layers of ghost cells. The fluid variables and properties are cell-centered.

59

Each cycle includes seven computational steps. The pressure, p is computed in the first step by using the equation of state. In the second step, $n+1$ cell-centered Lagrangian pressure, $p^{n+1^{L^c}}$, and $n+1$ face-centered fluxing velocity, $\bar{U}^{n+1^{*f}}$ are obtained by using a linear approximation to the pressure (implicit). In the third step, the face-centered pressure, $p^{n+1^{*f}}$, is computed by using the continuity of acceleration principle (explicit). In the fourth step, the sources of momentum and energy are calculated with Δp^{n+1^c} and $p^{n+1^{*f}}$. The sum of the time n Lagrangian values and the sources, m^{n+1^L}, $\left(m\bar{U}\right)^{n+1^L}$, e^{n+1^L}, are computed in the fifth step. In the sixth step, the advection of mass, momentum and energy is computed by using the face-centered fluxing velocities, $\bar{U}^{n+1^{*f}}$. Finally mass, momentum, and energy quantities calculated in step 5 are updated with the advection contribution calculated in step 6. Superscripts c and f denote cell-centered and face-centered quantities, respectively. The converged solution will be obtained by iteration of the above cycle.
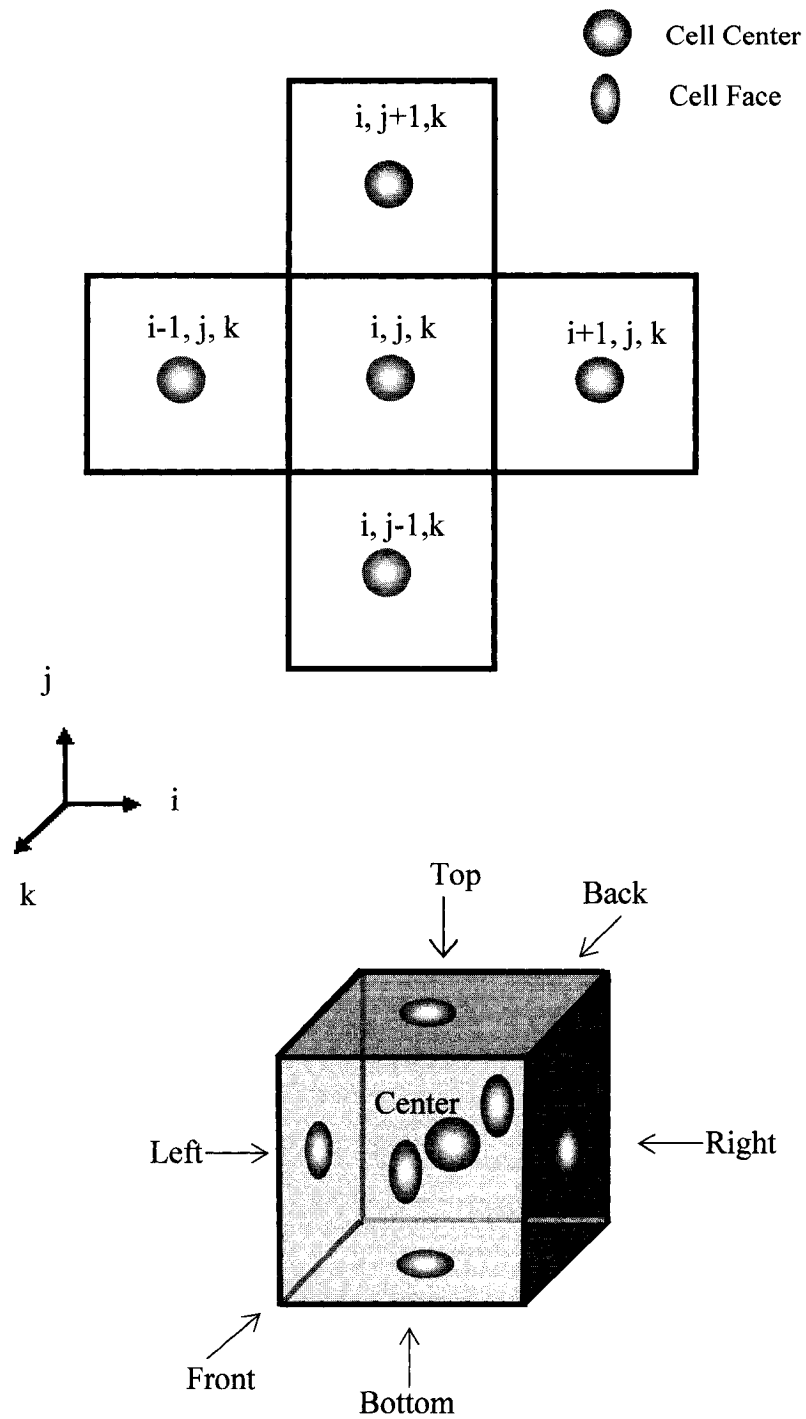
Figure 3-1   Grid arrangement and the cell face labeling

61

3.1.3. Inter-phase Momentum and Heat Exchange

The force acted on a single sphere particle moving in a fluid with a relative velocity to the flow can be obtained from equation .

$$\vec{F} = \frac{1}{2}\rho_c |\vec{U}_{rel}| \vec{U}_{rel} C_D A \tag{3.6}$$

where ρ_c presents the bulk density of the fluid (continuous phase), C_D denotes the drag force acting on a spherical particle, and A is the area of the sphere (subscripts c and d denotes continuous and dispersed phases, respectively).

The volume fraction occupied by N particles of the same size with a radius of r in unit volume is as follows:

$$\theta_d = (4/3)\pi r^3 N \tag{3.7}$$

Substituting the volume fraction obtained from equation (3.7) into equation (3.6), the total force acting on the particles per unit volume is derived:

$$\vec{f} = \rho_c |\vec{U}_{rel}| \vec{U}_{rel} C_D \theta_d (3/4r) \tag{3.8}$$

For multi fluids, the force can be presented as:

$$\vec{f}_{kl} = \sum_l \theta_k \theta_l K_{kl} (\vec{U}_l - \vec{U}_k) \tag{3.9}$$

where K is the momentum exchange coefficient.

For a two-phase flow, the coefficient can be expressed as:

$$K_{12} = K_{21} = (3/8)\frac{\rho_c}{\theta_c} C_D \frac{|\vec{U}_{rel}|}{r} \tag{3.10}$$

The heat exchange term of multi fluids is determined as follows:

62

$$\sum_{l} \theta_k \theta_l R_{kl} \left(T_l - T_k \right) \tag{3.11}$$

For a two-phase flow, the inter-phase energy exchange coefficient is:

$$R_{12} = R_{21} = \frac{\rho_c}{\theta_c} H_c \frac{\left| \vec{U}_{rel} \right|}{r} \tag{3.12}$$

where H_c is the convective heat transfer coefficient.

3.2. Model of the Cold Spray Process

In this section the numerical method of modeling a cold spray process with Eulerian approach is presented.

3.2.1. Nozzle Geometry and Boundary Conditions

Nozzle Geometry

The nozzle geometry used in the Eulerian approach is shown in Figure 3-2. The diameter of nozzle inlet and the particle inlet is 6 and 1 mm, respectively. The diameter of the nozzle throat and nozzle exit is 2 and 5.2 mm, respectively. The area ratio of the nozzle exit to throat is 6.76. The total nozzle length is 110 mm. The diverging section of the nozzle is 80 mm, which is much longer than that of nozzle converging section, 25 mm.
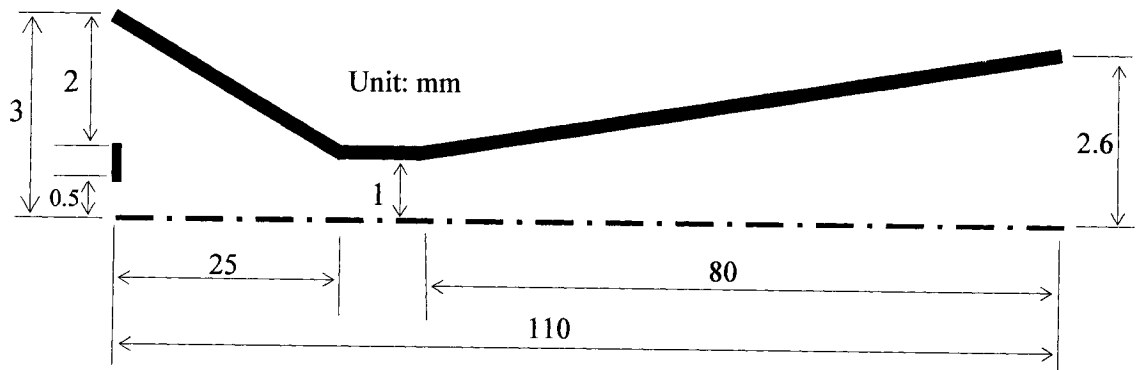
Figure 3-2   **Nozzle geometry and dimensions**

Boundary Conditions

The boundary conditions of the axisymmetric nozzle are shown in Figure 3-3. Helium is used as the carrier gas. At the nozzle inlet, the pressure and the temperature of the carrier gas are kept at 23 atm and 500 K, respectively. The gas pressure and temperature at the open boundary are 1 atm and 300 K, respectively. Twenty micron Copper particles are injected into the nozzle along the nozzle centreline. Simulations are conducted with various particle loadings in order to investigate the effect of particle volume fraction on the flow field.
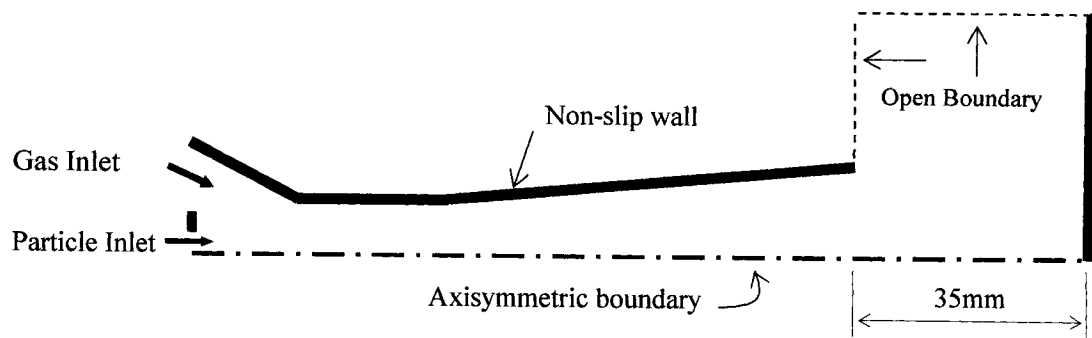
Figure 3-3   **Boundary conditions**

64

3.2.2. Discretization

In contrary to the case of using an Eulerian-Lagrangian method, mesh refinement will not result in more accurate solution when using Eulerian-Eulerian approach. Each single cell in the Eulerian approach should be large enough to contain sufficient number of particles so that the averages, such as the average volume fraction, mass, and energy can be calculated. If the size of control volume is too small, particulates can no longer be treated as continuum. On the other hand, a coarse grid will downgrade the accuracy of the calculation. To obtain a proper mesh size, many simulations have been carried out with various mesh sizes. For the given operating conditions, it is found that when the mesh size is about 0.2 x 0.2 mm, the numerical error due to the mesh size is within 1 %. Further increasing or decreasing the mesh size would either degrade the accuracy, or result in a diverging solution.

In the present work, the whole computational domain is composed of 6 blocks and 2 sections. There are 17 vertical nodes and 551 axial nodes inside the nozzle. The total numbers of the cells in the nozzle is 9365. In addition, the computational domain outside the nozzle is composed of 154 vertical nodes and 151 axial nodes. The total nodes located between the nozzle exit and the substrate is 23254 when the substrate stand-off distance is 30 mm. The numbers of nodes outside the nozzle varies with the stand-off distance of the substrate.

3.2.3. Numerical Techniques

CFDLib, a CFD open source developed by Los Alamos National Laboratory is used to solve the governing equations in the Eulerian-Eulerian approach [10], [11]. The

65

numerical scheme is finite volume with cell-centered state variables. The modular design of CFDLib enables it to perform multiphase and multifluid computations, both for incompressible and compressible flows.

A preprocessor is developed to generate 2-D axisymmetric geometries and the computational mesh. Helium is used as the carrier gas and is assumed to be an ideal gas. 20 μm copper particles are injected along with the carrier gas near the nozzle centreline. A k-ε turbulence model is used for this multifield compressible flow. Since the nozzle is axisymmetric and the particles are injected into the nozzle along the nozzle centreline, a 2-D axisymmetric model is used in this study in order to simplify the calculation.

3.3. Results and Discussions

3.3.1. Gas Phase

The gas Mach number contours of is shown in Figure 3-4. The gas is developed into sonic flow at the nozzle throat and further expands in the diverging section of the nozzle. The maximum gas velocity reaches about 2100 m/s at the nozzle exit. Three shock diamonds are formed between the nozzle exit and the substrate. A strong bow shock is also formed near the substrate.

66
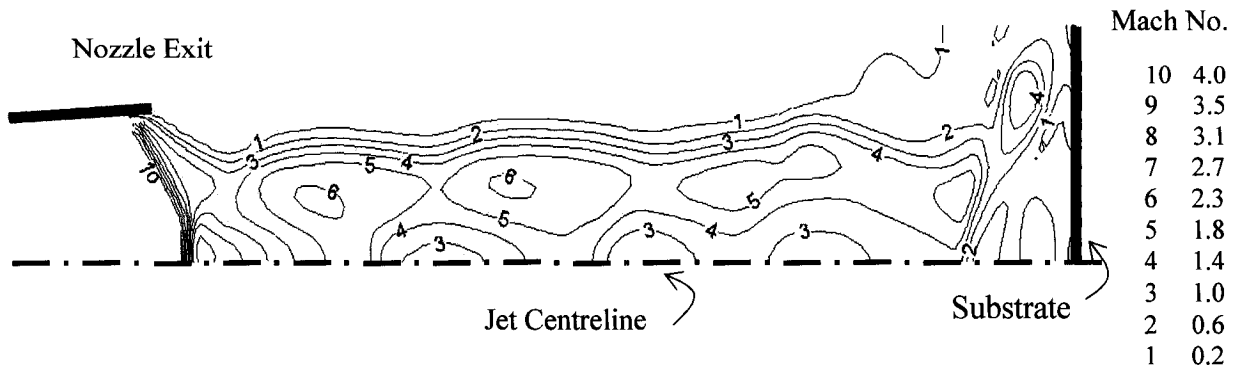
Figure 3-4   Mach contours of one phase flow

Near the injection point where the local particle loading* is rather high a dense particulate flow will be formed. Particles are accelerated by the gas flow and the dense particulate flow will be further developed near and along the nozzle centreline. Away from the nozzle centreline, particulate flow gradually becomes dilute. As the particulate flow is advancing through the nozzle, particle volume fraction will be decreased as shown in the Figure 3-5. The local dense particle flow near the nozzle centreline would augment the turbulence of the gas flow nearby.
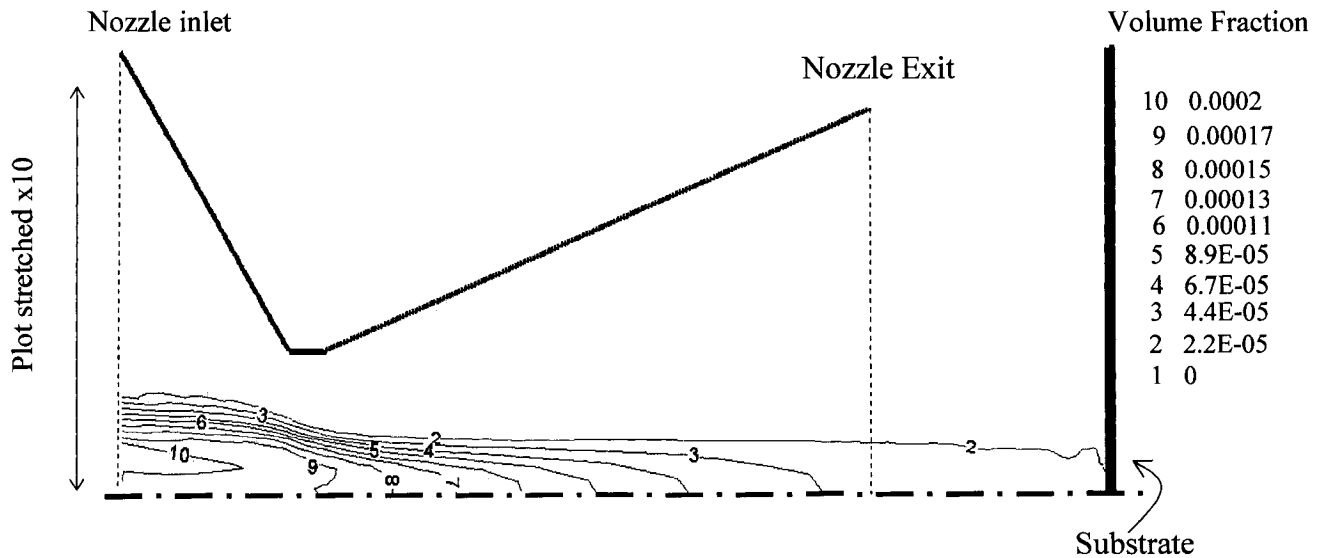
Figure 3-5   Particle volume fraction contours

---

* Loading is the ratio of the mass flows of the dispersed phase to that of the continuous phase.

The effect of particle loading (or volume fraction) on shocks and expansion waves is illustrated in Figure 3-6 as the local particle volume fraction at the inlet is increased from 0.0002 to 0.01. As shown in Figure 3-6 (a) when there is no particle injection, similar to the results of the Lagrangian approach a series of shocks and expansion waves (shock diamonds) are formed outside the nozzle with maximum and minimum Mach number located at the centreline. When copper particles are introduced to the nozzle with an inlet volume fraction of 0.0002, the local particle loading will be about 77% at the nozzle inlet boundary. As shown in Figure 3-6 (b), the subsonic areas which previously located between the shock diamonds start to connect with each other near the jet centreline. The shock diamonds are shifted away from the centreline area to the dilute flow area. Consequently, the supersonic flow near the jet centreline is turned to subsonic by the local dense flow. If the volume fraction at the particle inlet is increased to 0.0004 (local particle loading is increased to about 150 %), as shown in Figure 3-6 (c), the effect of particle volume fraction on the gas flow field is more distinct at the nozzle exit. As the volume fraction is increased to 0.0005 (local particle loading is increased to about 200 %), as shown in Figure 3-6 (d), the gas flow is significantly decelerated in such a way that the high speed flow cannot be further developed in the diverging section of the de Laval nozzle. This is due to the fact that the majority of the gas flow in the diverging section is subsonic and the diverging nozzle acts as a diffuser. At this particle loading the cold spray nozzle should fail to operate.

(a) *Particle volume fraction = 0 (Local loading =0)*

Nozzle Exit

Substrate

Mach No.

10	4.0
9	3.5
8	3.1
7	2.7
6	2.3
5	1.8
4	1.4
3	1.0
2	0.6
1	0.2

(b) *Particle volume fraction = 0.0002 (Local loading =77%)*

Nozzle Exit

Substrat

Mach No.

9	3.5
8	3.1
7	2.7
6	2.3
5	1.8
4	1.4
3	1.0
2	0.6
1	0.2

(c) *Particle volume fraction = 0.0004 (Local loading = 150%)*

Nozzle Exit

Substrat

Mach No.

9	3.5
8	3.1
7	2.7
6	2.3
5	2.0
4	1.6
3	1.2
2	0.8
1	0.5

(d) *Particle volume fraction = 0.0005 (Local loading =200%)*

Nozzle Exit

Substrat

Mach No.

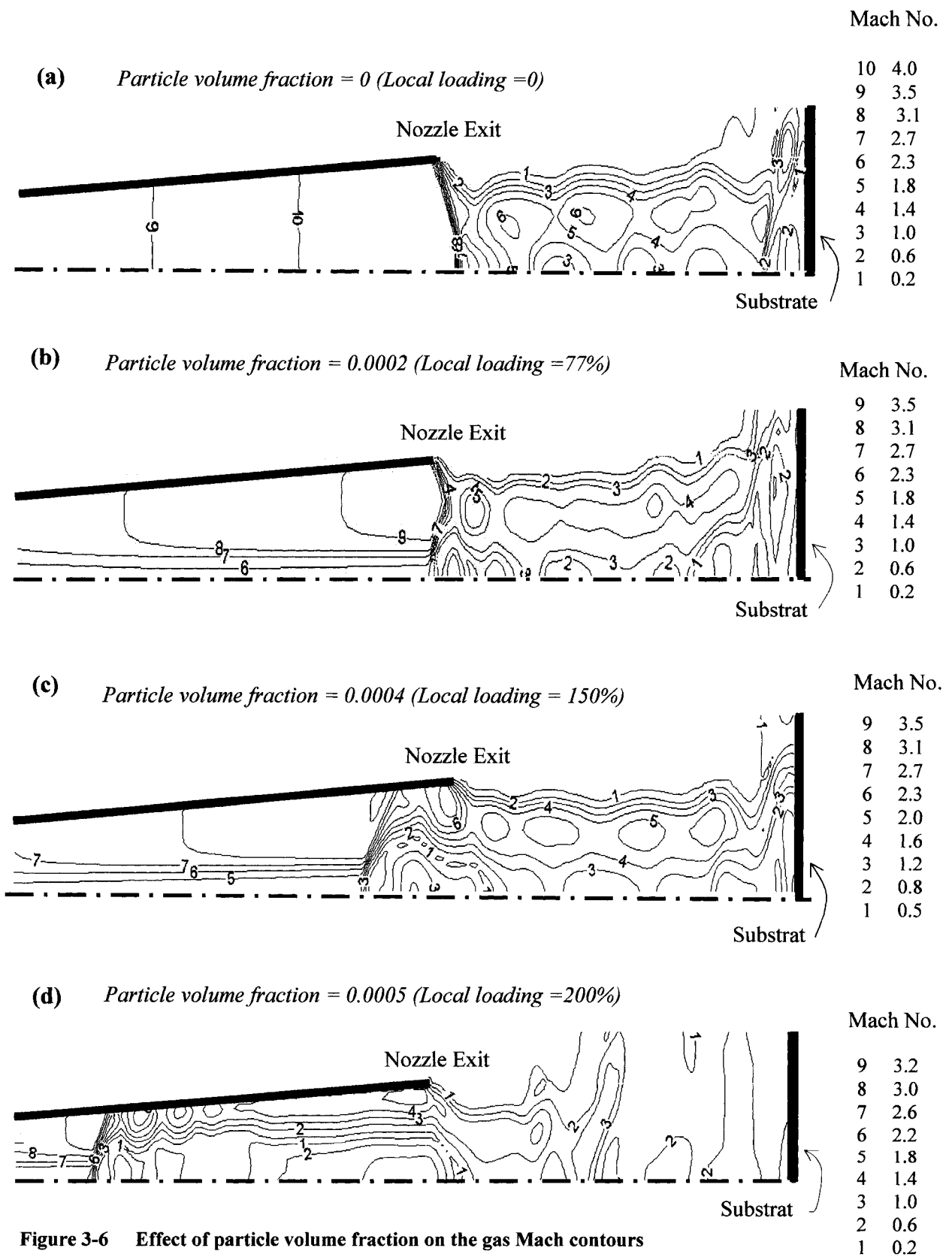|	
9	3.2
8	3.0
7	2.6
6	2.2
5	1.8
4	1.4
3	1.0
2	0.6
1	0.2

Figure 3-6   Effect of particle volume fraction on the gas Mach contours

69

3.3.2. Particle Phase

3.3.2.1. Effect of Dense Particle Flow on Particle Velocity Distribution

The local dense flow near the jet centreline not only affects the flow of the gas phase but also the particle velocity distribution. As shown in Figure 3-7 (a) and (b), the velocities of those particles in the shock diamonds area (about from 2 to 2.6 mm away from the jet centreline) are the largest because they are accelerated by the shocks. Velocity of the particles which are in the dense particulate flow area is small because of the negative effect of the local dense flow on the relative particle Mach number defined by equation (2.10). Since the relative Mach number of the particles in a dense flow is smaller than that in a dilute flow, the particles in the jet center are not sufficiently accelerated. In addition, the velocities of the particles which have dispersed to the subsonic dilute flow area outside the shock diamonds also decrease sharply. The kinetic energies of these particles dissipate quickly because of the viscous effect in the subsonic region. A similar particle velocity distribution as shown in Figure 3-7 (b) has also been observed in an experiment reported by Champagne et al. [33].

The effect of local dense flow on particle velocity can be further demonstrated as the volume fraction of the particles is increased. As shown in Figure 3-7 (b), when the particle volume fraction at the particle inlet is increased from 0.0004 to 0.001, the velocities of the particles upon impact decrease. Therefore, particle loading in the cold spray can significantly affect the particle velocity because of the negative effect of the local dense particulate flow on the gas flow regime by changing it from supersonic to

70

subsonic flow. It can also be observed in Figure 3-7 (b) that the velocity distribution of those particles in a dense flow is more uniform than that in a dilute flow. The particle-particle interaction and collisions in a dense flow tend to make the particle velocity distribution at different locations to be more uniform.

(a)

(b)

Distance from the jet centreline (mm)
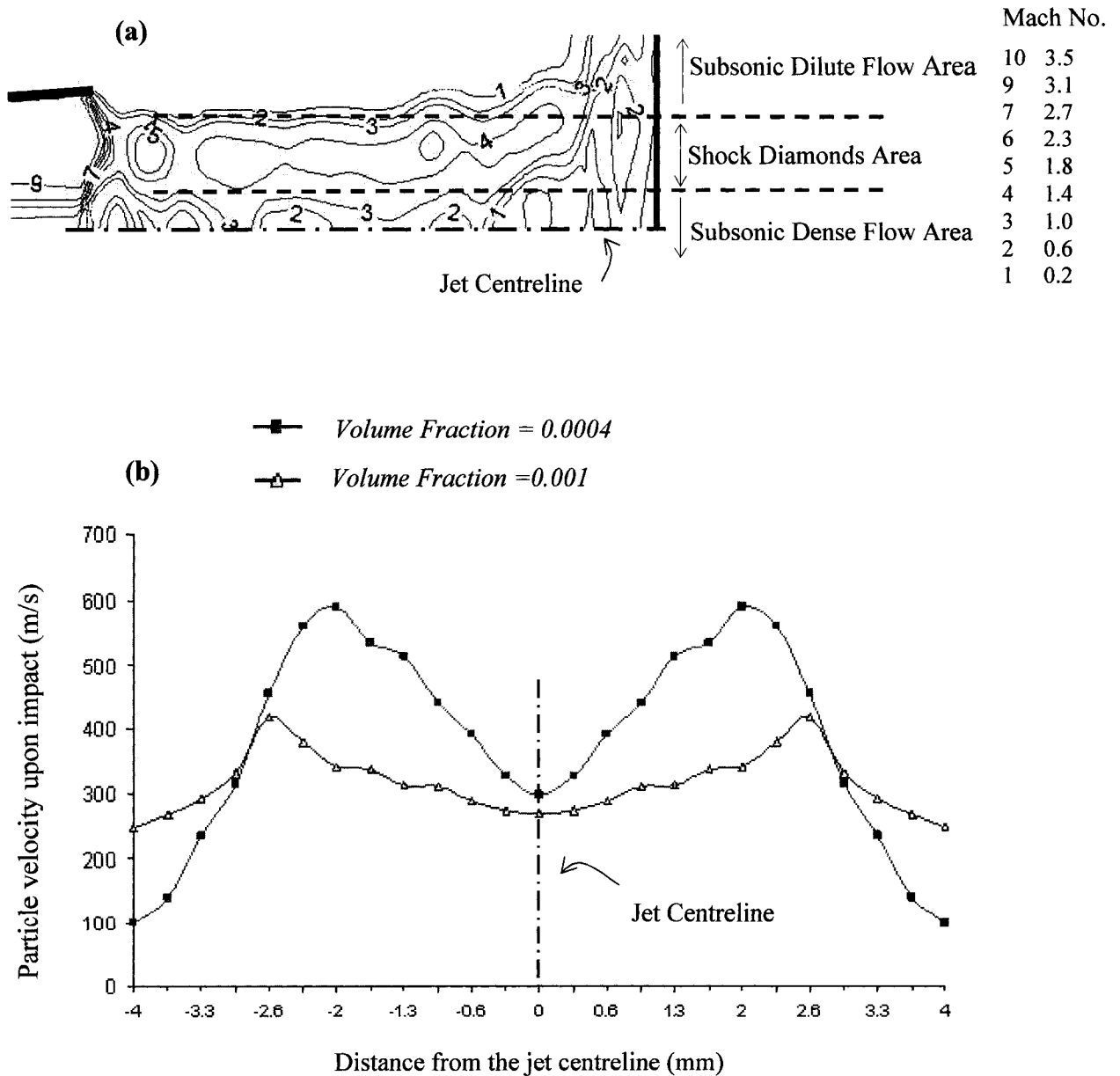
Figure 3-7   Effect of particle loading on particle velocity distribution upon impact (a) Dense flow, shock diamonds, and dilute flow areas in the gas jet (b) Particle velocity distribution away from the jet centreline

71

3.3.2.2. Effect of Bow Shock on Particle Velocity
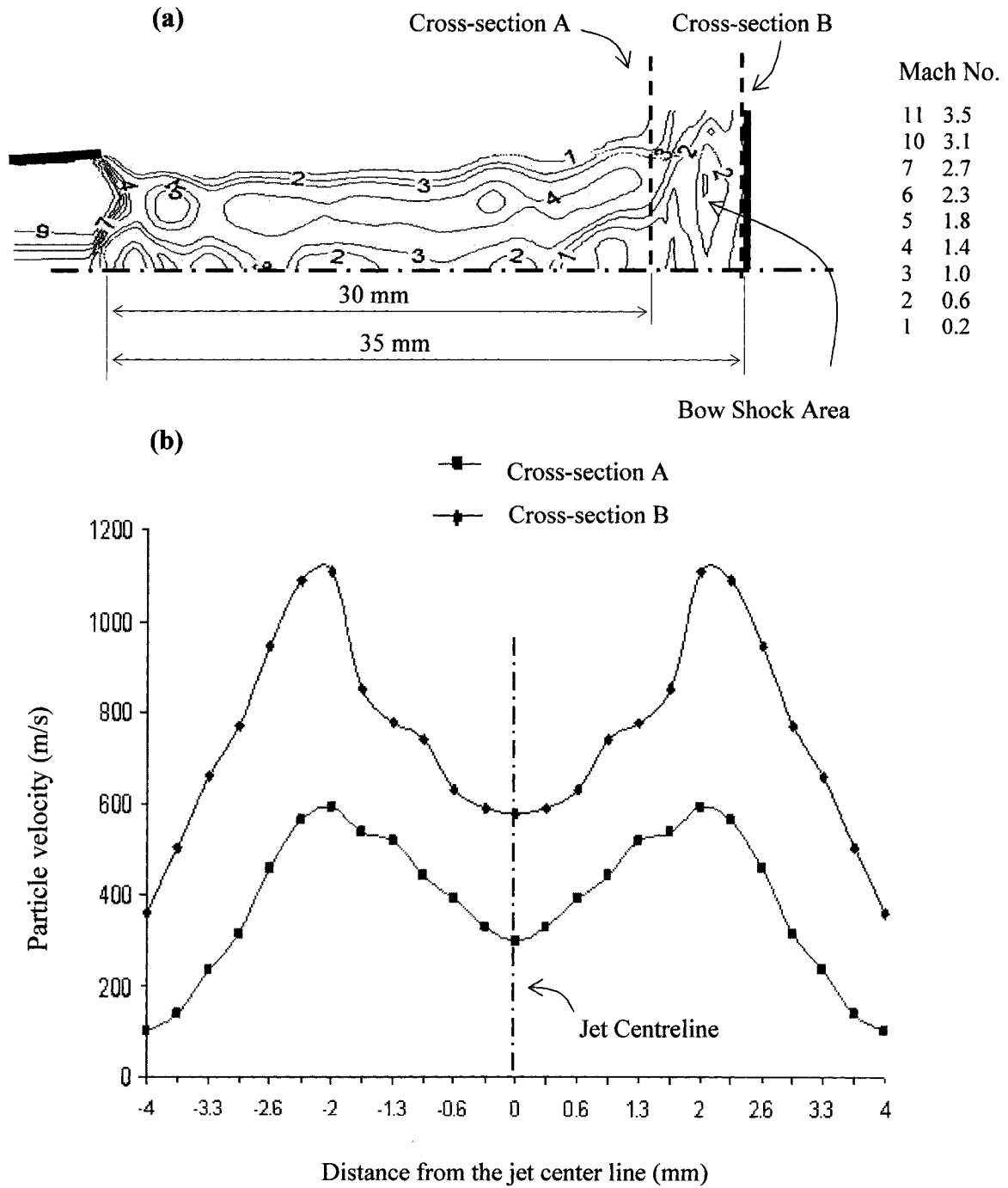
(a)

(b)

Figure 3-8 Effect of the bow shock on particle velocity (a) Particle velocity tracking position (b) Particle velocity before and after the bow shock

72

The effect of bow shock can also be observed when using an Eulerian approach. As it is demonstrated in Figure 3-8, particle velocities are calculated at two cross-sections; (a) prior to the bow shock, (b) adjacent to the substrate. Upstream of the bow shock, particle velocities are much higher than those upon impact. The particle velocity decreases sharply near the substrate because of the effect of the bow shock.

3.3.2.3. Effect of Particle Density on Particle Velocity upon Impact

Figure 3-9 shows the effect of particle density on the particle velocity upon impact. Two commonly used powders in the cold spray process are examined. The velocities of the aluminum particles are higher than those of the copper particles at the dense flow area and at the shock diamonds area. This is because the density of aluminum particles is lower than copper particles, resulting in smaller Stokes number for aluminum particles. Consequently, aluminum particles can be accelerated to higher velocities than the copper particles under the same operating condition. However, the velocity of aluminum particles decrease rapidly as it compares with copper particles at the subsonic dilute flow area because of their smaller Stokes number.
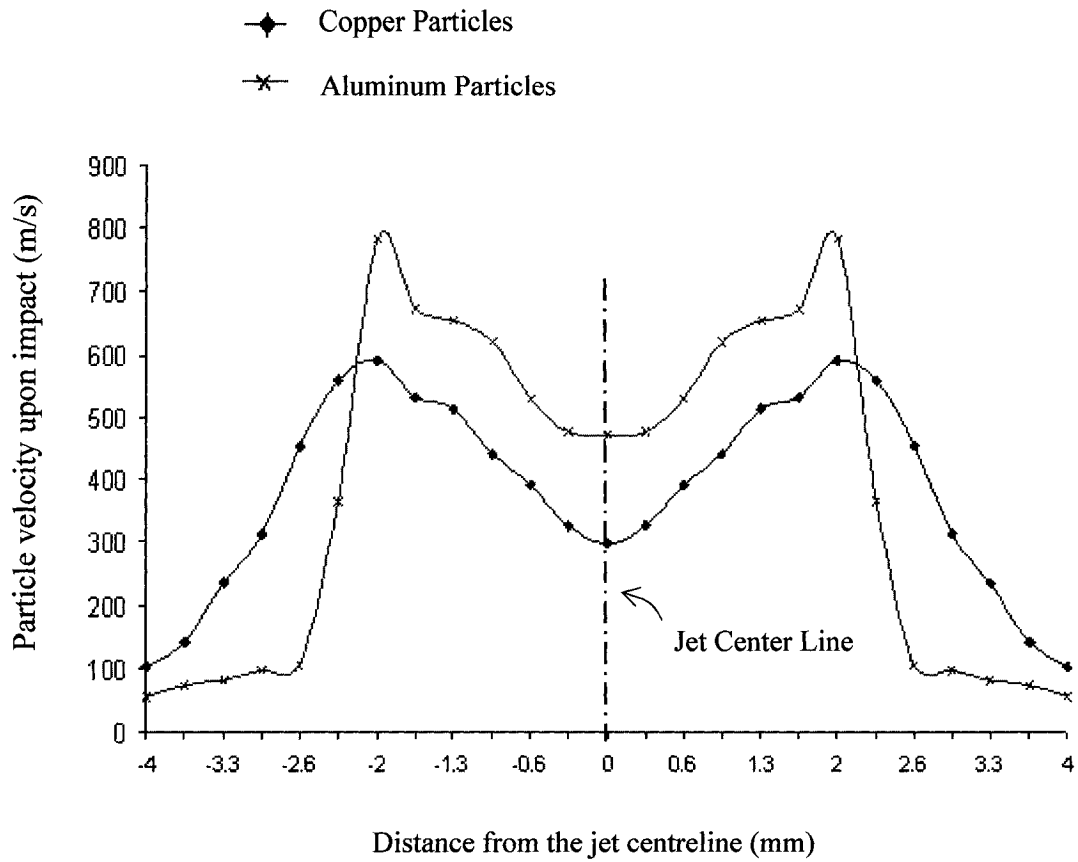
73

Figure 3-9   **Effect of particle material on particle velocity upon impact**

4. Closure

As mentioned in the previous chapters, cold spray process has been a focus of many studies because of its vast potential applications in various industries. However, most of the former research works focused on the study of the optimum operating conditions, such as the stagnation pressure and temperature, and the design of the nozzle. The present work analyzed the effect of shock diamonds and bow shocks on the normal velocity of the particle upon impact by using the Lagrangian particle tracking method [8 and 9]. In addition, the effects of particle size and substrate geometry on the particle velocity were studied. The Eulerian approach [10 and 11] was also used in parallel with the Lagrangian approach in order to investigate the effect of dense flow on the gas flow and on the particle velocity distribution.

4.1. Conclusions

In this study, the Lagrangian approach was first used to analyze the dilute particulate flow. The correlations of Igra and Takayama [26] and Henderson [27] were used to calculate particle normal velocity upon impact on a substrate. The conclusions from the Lagrangian approach include:

- Shock diamonds and a strong bow shock were observed in the gas flow, which were produced by interaction of Prantle-Meyer expansion waves and oblique shock waves outside the over-expanded supersonic nozzle. The number of

75

shocks observed in the numerical results depends on the stand-off distance of the substrate and the turbulence model. It was found that particle velocity increased in within the expansion waves while decreased through compression waves.

- It was demonstrated that particle normal velocity decreases noticeably near the substrate due to the formation of a strong bow shock. In addition, the existence of a stagnation core area between the bow shock and the substrate can turn particles away from the normal direction and result in a significant decrease in the particle normal velocity upon impact.

- Since Henderson correlation [27] is more sensitive to the shocks, especially to the bow shock, it was used to anticipate the optimum substrate location. The optimum substrate stand-off distance was found to be 11 mm for the applied operating conditions.

- Igra and Takayama correlation [26] was employed in this work to estimate the optimum particle size and the effect of the substrate geometry. The optimum particle size for copper particles was found to be about 35 μm for the applied operating conditions.

- It was also found that the effect of substrate geometry can significantly change the particle normal velocity upon impact. The mean normal velocity of small particles upon impact on a convex substrate is the largest as compared to that of the flat and the concave substrates because the strength of the bow shock near a convex substrate is the least. The value of the mean normal velocity of large

76

particles upon impact on the flat, concave, and convex substrates is close to each other. This is because of the large Stokes number associated with large particles which makes them less sensitive to the bow shock as compared to small ones.

The Eulerian approach [10 and 11] was also used in this study to analyze the dense particle flow in the cold spray process. The summary of the result of fully Eulerian approach is listed in the following items:

- Comparing to the Lagrangian approach, the interaction of the two phases of gas and solid particles in the Eulerian approach is captured not only by source terms in the momentum and energy equations, but also by the volume fraction term. The fully Eulerian approach can analyze the change in average density of each phase at each control volume with the volume fraction term in the conservation laws.

- In the Eulerian-Eulerian approach, it was found that most particles are concentrated in the area near the jet centreline where the coating particles are injected to the nozzle. The local dense particle flow near the centreline can significantly affect the nearby gas flow. The velocity of the gas flow near the centreline of the jet is less than that of the gas flow away from the centreline, where the flow remained a dilute particle flow. The shock diamonds were also found shifted away from the jet centreline because of the presence of the dense particulate flow near the centreline.

77

- The dense particulate flow near the jet centreline also negatively affects the particle velocity. Since the relative Mach number near the centreline is smaller than that of outside area, the particles in the jet center are not sufficiently accelerated. It was observed in the simulation that the impact velocities of the particles near the centreline were smaller than those particles traveling away from the centreline. Obviously, the deposition efficiency of particles will decrease significantly if the local particle loading exceeds is rather high. For example, for the presented operating conditions, the nozzle is functional when the local loading does not exceed 150%.

- It was also found that the impact velocity of those particles traveling through deflected shock diamonds is rather high. These particles are accelerated by the shock waves. However, when some particles are dispersed far away from the nozzle centreline, they are decelerated in the subsonic area outside the shock diamond areas.

All the factors mentioned above can significantly affect particle normal velocity upon impact. Since particle normal velocity upon impact is the most important factor affecting the coating deposition efficiency, studying these factors with both the Lagrangian and Eulerian approaches will allow us to better understand the physics governing the complex high speed gas-particle flow in the cold spray process. Finally, the deposition efficiency and coating quality can be improved.

4.2. Future Works

The present work has analyzed the effect of shocks and substrate geometry in the cold spray process by using various drag coefficient models in the Lagrangian approach. The effect of dense particle flow has also been studied with fully Eulerian approach. Some primary results and conclusions have been obtained. The calculated mean particle velocity was very close to the experimental data provided by NRC-IMI. However, more work should be carried out using both methods in order to thoroughly understand these effects. The future works are recommended as follows:

- The simulation results of this work have been partly validated by the experimental results provided by NRC-IMI. Further validation works are required in order to obtain not only the accurate mean particle velocity but also the similar particle velocity standard deviation.

- The area ratio of the nozzle exit to the nozzle throat is 6.75 in this study. This area ratio is so large that the Mach number at the nozzle exit can reach up to 4.3. However, it is reported by Jodoin [16] that the Mach number should not be greater than 4 because of the negative effect of the shocks at high Mach number. In future, the simulation work should be conducted with a nozzle of smaller area ratio.

- Igra and Takayama correlation [26] and Henderson correlation [27] have been used in the Lagrangian approach. These correlations can estimate the effect of the bow shock on the particle normal velocity upon impact. However, when the nozzle geometry or the operating conditions are changed, these correlations may

79

no longer be the optimum drag model to accurately predict the particle velocity. This is because each drag law has its range of application, depending on the particle Reynolds number, Mach number, and shape. More drag correlations should be tried in the future in order to find an optimum drag correlation which can predict not only accurate mean particle velocity but also correct velocity standard deviation. Obviously, experimental results will be very important in the process of validating an appropriate drag law to simulate cold spray process.

- Since the nozzle in this thesis is axisymmetric and the particles are injected from the nozzle centreline, two-dimensional model was used to simulate the cold spray process. However, there are many cold spray nozzles in which particles are injected into the nozzle from the nozzle wall, such as that in the experiments of NRC-IMI. In the future the study should be carried out with a 3-D model in order to predict the particle landing position more accurately.

- Some primary results have been obtained by using the fully Eulerian approach with the CFDLib codes. In the future the drag correlation used in CFDLib can be changed to obtain more accurate particle velocity. The turbulence model of CFDLib codes is k-ε model. In future this model can also be changed to other models to facilitate capturing the shocks and expansion waves more accurately.

References

[1]   J. H. Zaat, A quarter of a century of plasma spraying, Ann. Rev. Mater. Sci. 1983, 13:9-42

[2]   L. Pawlowski, The science and engineering of thermal spray coatings, John Wiley and Sons, Cichester, UK, 1995

[3]   A.P. Alkhimov; A.N. Papyrin, V.F. Kosarev, N.I. Nesterovich, and M.M. Shushpanov, Gas Dynamic Spraying Method for Applying a Coating, U.S. Patent Number: 5 302 414, April 12, 1994, p1-16.

[4]   D.L. Gilmore, R.C. Dykhuizen, R.A. Neiser, T.J. Roemer, and M.F. Smith, Particle Velocity and Deposition Efficiency in the Cold Spray Process, Journal of Thermal Spray Technology, Volume 8(4), 1999, p576-582.

[5]   R.C. Dykhuizen and M.F. Smith, Gas Dynamic Principles of Cold Spray, Journal of Thermal Spray Technology, Volume 7(2), 1998, p205-212.

[6]   C.J. Li, W.Y. Li, and Y.Y. Wang, Effect of Spray Angle on Deposition Characteristics in Cold Spraying, Thermal Spray: Advancing the Science and Applying the Technology, B.R. Marple and C. Moreau, Ed., May 5-8, 2003 (Orlando, FL), ASM International, 2003, p91-96.

[7]   V. Champagne, D. Helfritch, P. Leyman, R. Lempicki, S. Grendahl, The Effect of Gas and Metal Characteristics on Sprayed Metal Coatings, Modeling Simul. Mater. Sci. Eng. 13, 2005, p1119-1128.

[8]   R. Davis, R. Pfeffer, M. Roco, and B. Ennis, First International Particle Technology Forum, Denver, CO:AIChE, 1994

[9]   C. T. Crowe, M. P. Sharma, and D. E. Stock, The Particle-Source-in-Cell (PSI-CELL) for gas droplet flows, Journal of Fluid Engineering, 1977, 99:325-31.

[10]   A. Dolatabadi, J. Mostaghimi, and V. Pershin, Modeling Dense Suspension of Solid Particles in Highly Compressible Flows, International Journal of Computational Fluid Dynamics, Volume 18, Number 2, 2004, p125-131.

[11]   C. T. Crowe, The state-of-the-art in the development of numerical models for dispersed phase flows, Proceedings of International Conference on Multiphase Flows, Tsukuba, Japan, 1991, 3:49-60.

[12]   D. A. Drew, R. T. Lahey, Analythical modeling of multiphase flow, In Particulate Two-Phase Flow, ed. MCRoco, 1993, Chap. 16, p 509-66

[13]   C. T. Crowe, Review-Numerical models for Dilute Gas-Particle Flows, J. Fluids Eng. 1982, Vol. 104/297,

[14]   S.E. Elghobashi, On predicting particle-laden turbulent flows, appl. Sci. Res. 1994, 52:309-29.

[15]   L. S. Fan and C. Zhu, Principles of Gas-Solid Flows, Cambridge University Press, 1998

[16]   B. Jodoin, Cold Spray Nozzle Mach Number Limitation, Journal of Thermal Spray Technology, Volume 11(4) December 2002, p 496-507.

[17]   W.Y. Li, C.J. Li, Optimal Design of a Novel Cold Spray Gun Nozzle at a Limited Space, Journal of Thermal Spray Technology, Volume 14 (3) September 2005, p391-396.

[18]   T. Han, Z. Zhao, B. A. Gillispie, J. R. Smith, Effects of Spray Conditions on Coating Formation by the Kinetic Spray Process, Journal of Thermal Spray Technology, Volume 14 (3) September 2005, p373-383.

[19]   A. Dolatabadi, J. Mostaghimi, and V. Pershin, Effect of Cylindrical Shroud on Particle in High Velocity Oxy-fuel Spray Process, Science and Technology of Advanced Materials, 3 (2002), 2002, p 245-255.

[20]   A. Dolatabadi, J. Mostaghimi, and V. Pershin, A New Attachment for Controlling Gas Flow in HVOF Process, Journal of Thermal Spray Technology, Volume 14(1), 2005, p91-99.

[21]   A. Dolatabadi and J. Mostaghimi, Effect of Flow Regime on Deposition Efficiency in the High Velocity Oxy-Fuel (HVOF) Process, Canadian Ceramics Society 99th Annual Technical Forum, Journal of the Canadian Ceramic Society, Volume 70, September 2001, p 37.

[22]   A. Dolatabadi, J. Mostaghimi, and V. Pershin, High Efficiency Nozzle for Thermal Spray of High Quality, Low Oxide Content Coatings, U.S. Patent Number 6,845,929, January 2005.

[23]   B. E. Launder, G. J. Reece, and W. Rodi, Progress in the Development of a Reynolds-Stress Turbulence Closure, J. Fluid Mech., 68(3) April 1975, p537-566.

83

[24]   M. M. Gibson, B. E. Launder, Ground Effects on Pressure Fluctuations in the Atmospheric Boundary Layer, J. Fluid Mech., 1978, 86: p491-511.

[25]   W.E. Mallard, F. Westley, J.T. Herron, R.F. Hampson, NIST chemical kinetics database 17, NIST Standard Reference Data, Gaithersburg, MD, 1994

[26]   Igra, O. and Takayama, K., Shock Tube Study of the Drag Coefficient of a Sphere in a Non-Stationary Flow, R. Soc. Land. A Proc., 442 ( ), 1993, p231-2467

[27]   C.B. Henderson, Drag Coefficients of Spheres in Continuum and Rarefied Flows, AIAA Journal, Vol 14 (No. 6), 1976, p707-708

[28]   C. Moreau, P. Gougeon, M. Lamontagne, V. Lacasse, G. Vaudreuil, P. Cielo, On-line Control of the Plasma Spraying Process by Monitoring the Temperature, Velocity and Trajectory of In-flight Particles, Proceeding of the 7th NTSC, Boston, Massachusetts, USA, 1994, p 431-437.

[29]   G. Rudinger, Fundamentals of Gas-Particle Flow, Volume 2, Elsevier Scientific Publishing Company, 1980.

[30]   B.A. Kashiwa, Statistical theory of turbulent incompressible multimaterial flow. Technical Report LA-11088-T, Los Alamos National Laboratory, 1987.

[31]   B.A. Kashiwa, N. T. Padial, R.M. Rauenzahn, and W. VanderHeyden, A cell-centered ice method for multiphase flow simulations. Technical Report LA-UR-93-3922, Los Alamos National Laboratory, 1994.

[32]   W.B. VanderHeyden and B.A. Kashiwa, Compatible fluxes for van leer advection. *Journal of Computational Physics,* 1998, 146, 1–28.

[33]   V. K. Champagne, J. D. Helfritch, P. Leyman, S. Grendahl, B. Klotz, Interface Material Mixing Formed by the Depostion of Copper on Aluminum by Means of

the Cold Spray Process, Journal of Thermal Spray Technology, Volume 14(3) September 2005, p330-334.